Nat. Hazards Earth Syst. Sci., 21, 3465–3487, 2021
https://doi.org/10.5194/nhess-21-3465-2021

Natural Hazards and Earth System Sciences
Open Access
EGU

Main Ethiopian Rift landslides formed in contrasting geological settings and climatic conditions

Karel Martínek[1,2], Kryštof Verner[2,3], Tomáš Hroch[2], Leta A. Megerssa[3,2], Veronika Kopačková[2], David Buriánek[2], Ameha Muluneh[4], Radka Kalinová[3], Miheret Yakob[5], and Muluken Kassa[4]

[1]Institute of Geology and Palaeontology, Faculty of Science, Charles University, Albertov 6, Prague 12843, Czech Republic
[2]Czech Geological Survey, Klárov 3, 11821 Prague, Czech Republic
[3]Institute of Petrology and Structural Geology, Faculty of Science, Charles University, Albertov 6, Prague 12843, Czech Republic
[4]School of Earth Sciences, Addis Ababa University, Arat Kilo, 1176 Addis Ababa, Ethiopia
[5]Geological Survey of Ethiopia, P.O. Box 2302, Addis Ababa, Ethiopia

Correspondence: Karel Martínek (karel.j.martinek@gmail.com)

Received: 18 December 2020 – Discussion started: 18 January 2021
Revised: 20 September 2021 – Accepted: 7 October 2021 – Published: 16 November 2021

Abstract. The Main Ethiopian Rift (MER), where active continental rifting creates specific conditions for landslide formation, provides a prospective area to study the influence of tectonics, lithology, geomorphology, and climate on landslide formation. New structural and morphotectonic data from central Main Ethiopian Rift (CMER) and southern Main Ethiopian Rift (SMER) support a model of progressive change in the regional extension from NW–SE to the recent E(ENE)–W(WSW) direction, driven by the African and Somali plates moving apart with the presumed contribution of the NNE(NE)–SSW(SW) extension controlled by the Arabian Plate. The formation and polyphase reactivation of faults in the changing regional stress field significantly increase the rocks' tectonic anisotropy, slope, and the risk of slope instabilities forming.

According to geostatistical analysis, areas prone to landslides in the central and southern MER occur on steep slopes, almost exclusively formed on active normal fault escarpments. Landslide areas are also influenced by higher annual precipitation, precipitation seasonality, vegetation density, and seasonality. Deforestation is also an important predisposition because rockfalls and landslide areas typically occur on areas with bushland, grassland, and cultivated land cover.

A detailed study on active rift escarpment in the Arba Minch area revealed similar affinities as in a regional study of MER. Landslides here are closely associated with steep, mostly faulted, slopes and a higher density of vegetation. Active faulting forming steep slopes is the main predisposition for landslide formation here, and the main triggers are seismicity and seasonal precipitation. The Mejo area situated on the uplifting Ethiopian Plateau 60 km east of the Great Rift Valley shows that landslide occurrence is strongly influenced by steep erosional slopes and a deeply weathered Proterozoic metamorphic basement. Regional uplift, accompanied by rapid headward erosion forming steep slopes together with unfavourable lithological conditions, is the main predisposition for landslide formation; the main triggers here are intense precipitation and higher precipitation seasonality.

1 Introduction

Slope instabilities, including mainly landslides, rockfalls, and debris flows are usually influenced by key factors such as slope, bedrock lithology and rock fabric anisotropy, active tectonics and seismicity, type and grade of weathering, climatic conditions, vegetation cover, land use, and human activity. Links between these factors and the formation of landslides and rockfalls are complex (e.g. Abebe et al., 2010; Meinhardt et al., 2015). Geomorphic indices have been used to decipher links between landform and tectonics in several studies (Ayalew and Yamagishi, 2004; Ayalew et al., 2004). However, the influence of other factors on slope instabilities

is unclear and a matter of current debate (e.g. Asfaw, 2007; Temesgen et al., 1999; Vařilová et al., 2015; Woldearegay, 2013). In general, ongoing discussions on the formation of slope instabilities in an active rift setting state either tectonics, climate, or anthropogenic activity as being triggering factors, depending on the characteristic conditions at the particular locality (e.g. Mancini et al., 2010; Peduzzi, 2010; Wotchoko et al., 2016). Other studies also conclude that lithology and precipitation are the main landslide controlling factors (e.g. Kumar et al., 2019, and references therein). Geomorphic indices, such as slope, aspect, hypsometric integral, the stream length gradient index, or river incision rates, are capable of detecting landform responses to tectonics (Ayalew and Yamagishi, 2004; Gao et al., 2013), but studies showing slope instabilities having a direct link to active tectonics are relatively rare (Chang et al., 2018, and references therein). Other studies also conclude that lithology and precipitation are the main landslide controlling factors (e.g. Kumar et al., 2019, and references therein).

Central and southern parts of the Main Ethiopian Rift (MER), which belong to the northern part of the East African Rift System (EARS), form a relatively narrow, slowly spreading extensional zone with a humid, strongly seasonal climate. The rift valley is significantly drier in comparison to the more humid rift flanks and plateau. There is a thick sequence of unconsolidated, often strongly weathered, volcaniclastic deposits cropping out in grabens on steep tectonic slopes or occasionally also on moderately elevated areas. Such a complex environment is an excellent natural laboratory to study the interplay of factors influencing various types of slope instabilities as they form in different geological and geomorphic conditions. Active extensional tectonism has a strong influence on the present-day morphology, but there are also important variations in climatic parameters (annual precipitation and seasonality); moreover, a population explosion in the last few decades has led to extensive deforestation, overgrazing, and dramatic changes in land cover and land use, which all may have significant importance in landslide formation (FAO, 2001; Janetos and Justice, 2000; Gessesse, 2007; Gete and Hurni, 2001; Melese, 2016).

This multidisciplinary study is focused on evaluating the landslide distribution in the central and southern MER. A combination of the results of geological, geohazard, and structural mapping, with remotely sensed data, and climatic, vegetation, and land use indicators is assessed using geostatistical methods. The discussion of the main factors influencing the formation of landslides in the regional scale in the central and southern MER and also on a detailed scale in the Mejo and Arba Minch areas in the southern part of the MER is the main focus of this study. In the regional-scale study, the direct link to tectonics is clear, so a large data set of new field structural data from this area is given. The situation in detailed scale studies in Mejo and Arba Minch is more complex. These two areas have contrasting styles of tectonic setting and varying lithological and climatic conditions, i.e. the Mejo landslide area is more humid, located on the eastern plateau, 60 km east of the rift valley, and dominated by highly weathered Proterozoic basement rocks, while the Arba Minch landslide area is situated directly on the western rift escarpment, with active tectonism and seismicity, and dominated by Tertiary volcanic rocks (Fig. 1). In both areas, slope failures are closely associated with steep slopes, but these are generated by very different processes, i.e. either active rift normal faulting or deep headward river erosion of the uplifting rift flank. The anthropogenic influence is also discussed, but only locally, because the relevant data for a thorough geostatistical evaluation are, unfortunately, missing.

2 Geological and geohazard setting

2.1 Geology and tectonics of the studied area

The overall geological pattern of southern Ethiopia includes a basement formed by metamorphic rocks of the Neoproterozoic age, which have been overlain by widespread volcanic sequences ranging from pre-rift Cenozoic volcanism to the Main Ethiopian Rift (MER) associated volcanism (Bonini et al., 2005; Hayward and Ebinger, 1996; Woldegabriel et al., 2000). The Precambrian rocks exposed in southern Ethiopia constitute the most southern part of the Arabian–Nubian Shield (ANS), which includes several terrane assemblages (for a review, see Fritz et al., 2013, and references therein). The ANS is an assemblage of juvenile low-grade volcano–sedimentary rocks and associated plutons and ophiolite traces with ages between ~ 890 and 580 Ma (Fritz et al., 2013). The Main Ethiopian Rift (MER) is an active intracontinental rift bearing the magma-dominated extension of the African (Nubian), Somali, and Arabian lithospheric plates (e.g. Acocella, 2010; Agostini et al., 2011). Of the MER reflecting temporally and spatially different stages of regional extension and volcanic activity, the following three segments have been defined (e.g. Hayward and Ebinger, 1996; Muluneh et al., 2014): (a) the northern Main Ethiopian Rift (NMER), (b) the central Main Ethiopian Rift (CMER), and (c) the southern Main Ethiopian Rift (SMER; see Fig. 1). In the southern part of the MER, the current rate of $\sim$E–W oriented extension between the African and Somali plates amounts to 5.2 ± 0.9 mm per year (Saria et al., 2014).

The volcanic activity in the studied parts of the CMER (Hossana area) and SMER (Dilla area) could be divided into three major episodes (Bonini et al., 2005; Corti, 2009; Hayward and Ebinger, 1996). The Eocene to Oligocene pre-rift volcanic products (~ 45 to 27 Ma) comprise mainly tholeiite to alkaline basalt lava flows and the associated volcaniclastic deposits (Amaro–Gamo Basalts), with the presence of rhyolite ignimbrites (Shole Ignimbrites) and minor trachytes (Burianek et al., 2018; Verner et al., 2018c, d). The Miocene syn-rift volcanic products (~ 22 to 8 Ma) are represented by basalts, felsic volcanites, and volcaniclastic rocks

(rhyolite lava, minor ignimbrites, trachyte lava flows, and related pyroclastic deposits) belonging mainly to the Getra and Kele sequences, including Mimo trachyte (Bonini et al., 2005; Ebinger et al., 1993, 2000). These two events were followed by a period of drastically low volcanism, except for a small eruption of peralkaline pantelleritic ignimbrites intercalated with minor basaltic lava flows in the areas beyond the rift escarpments (Bonini et al., 2005; see also Fig. 4). Subsequently, the products of Pleistocene to Holocene post-rift volcanic activity ($\sim$ 1.6–0.5 Ma) are bimodal volcanites and volcanoclastic rocks such as, for example, massive Nech Sar basalts, rhyolites, strongly welded rhyolitic ignimbrites, and other pyroclastic deposits (Ebinger et al., 1993). A typical example of post-rift volcanic activity in the southern CMER is the lower Pleistocene formation of unconsolidated pyroclastic deposits on the rift floor (e.g. Corbetti volcanic system; Rapprich et al., 2014), which was consequently disturbed by tectonic movements and erosion.

The complex fault pattern of the MER (interference of SSW(SW)–NNE(NE), N–S, and WNW(W)–ESE(E) trending faults) has been attributed to various mechanisms of contrasting hypothesis (for a review, see Abate et al., 2015; Erbello and Kidane, 2018), including (a) the pure extension orthogonal to the rift, (b) a right lateral NW–SE to the NNW–ESE transtension continuously transferred to sinistral oblique rifting as a result of an E–W regional extension, (c) a constant NE(ENE)–SW(WSW) trending extension, (d) a constant extension in the NW–SE direction, and (e) a constant E–W to ESE–WNW extension.

2.2 Geohazards in the central and southern MER

Active extensional tectonics and the intense volcanism associated with the East African Rift System (e.g. Agostini et al., 2011; Chorowicz, 2005) represent one of the main reasons for frequent hazardous geological phenomena in the Main Ethiopian Rift (MER). Characteristic rift-related morphology, seasonal climatic conditions, and inappropriate human interference in the landscape create suitable conditions for hazardous geological processes. Endogenous risk factors such as earthquakes, volcanism, and post-volcanic phenomena are closely related with tectonics in this area. The geomorphology is highly variable across the MER and is mainly the result of volcanic and tectonic events with the associated erosional and depositional processes (Billi, 2015).

Notable geohazard features across and along the MER range from intense erosion to slope-instability-related mass wasting processes, including rockfalls and debris flows up to shallow and deep-seated landslides, all with immense costs in terms of casualty and infrastructure loss (Abebe et al., 2005; Ayalew, 1999; Hearn, 2018). Landslides are rather more common in the highlands of Ethiopia. The most affected regions are the Blue Nile Gorge (Ayalew and Yamagishi, 2004; Gezahegn and Dessie, 1994; JICA and GSE, 2012; Tadesse, 1993), the Dessie area and the highlands surrounding Ambassel and Woldia (Ayenew and Barbieri, 2005; Fubelli et al., 2008), the Simien highlands, particularly western and central Tigray, the Sawla and Bonga areas of southern Ethiopia (Lemessa et al., 2000) and the MER margins of the western and eastern escarpment (Kycl et al., 2017; Rapprich and Eshetu, 2014; Rapprich et al., 2014; Temesgen et al., 2001), the surroundings of Finchewa, and the Debre Libanos and the Mugher locality (Zvelebil et al., 2010). On the western escarpment of the MER, a vast and recurrent landslide is notable close to the town of Debre Sina at the locality of Yizeba Weyn in central Ethiopia (Kropáček et al., 2015).

Other common geological hazards that recurrently appear in the area are ground fissures in various sectors along the rift floor, for example, north of the Fentale area in the northern MER (Williams et al., 2004) and various localities in the central MER segment (Asfaw, 1982, 1998; Ayalew et al., 2004) which often transform into deep and long gully systems (Billi and Dramis, 2003). Persistent seismic tremors, usually of lower magnitudes, are apparently located in the entire rift floor (e.g. Wilks et al., 2017). Particular clusters and source zones have been identified in Ethiopia, with those being (1) the western plateau margin, (2) the central Afar, (3) the Aisha block, (4) the Ankober area, (5) the central Main Ethiopian Rift, and (6) the southwestern Main Ethiopian Rift (Ayele, 2017). Nevertheless, historical high-magnitude earthquake records have also been reported (Asfaw, 1992; Gouin, 1975, 1979; Wilks et al., 2017). An updated probabilistic seismic hazard analysis and zonation has since been recently carried out with seismotectonic source zones constrained from recent studies for the Horn of Africa with reference to the East African Rift Valley (Ayele, 2017).

In addition to the seismic tremors, volcanism is also of apparent risk. Among the recent events are the Nabro Volcano in 2011 in the far northern part of the Afar Triangle (Goitom et al., 2015) and the Debahu rifting and volcanic dyke swarm intrusion events in 2005 (Ayele et al., 2007, 2009). These two events each triggered major alarms significant enough to warrant flight diversions (in the case of the Nabro Volcano) across the region and the temporary displacement of local people (e.g. Goitom et al., 2015).

3 Methods and data

Field geological, structural, geomorphological, and engineering geological mapping were conducted to acquire geological, tectonic, geomorphological, and rock mechanic properties (rock mass strength) characteristics.

3.1 Geotechnical data

Rock mass strength is obtained from the engineering geological map of the Hossana map sheet (Yekoye et al., 2012) and Dilla map sheet (Habtamu et al., 2012). The maps are

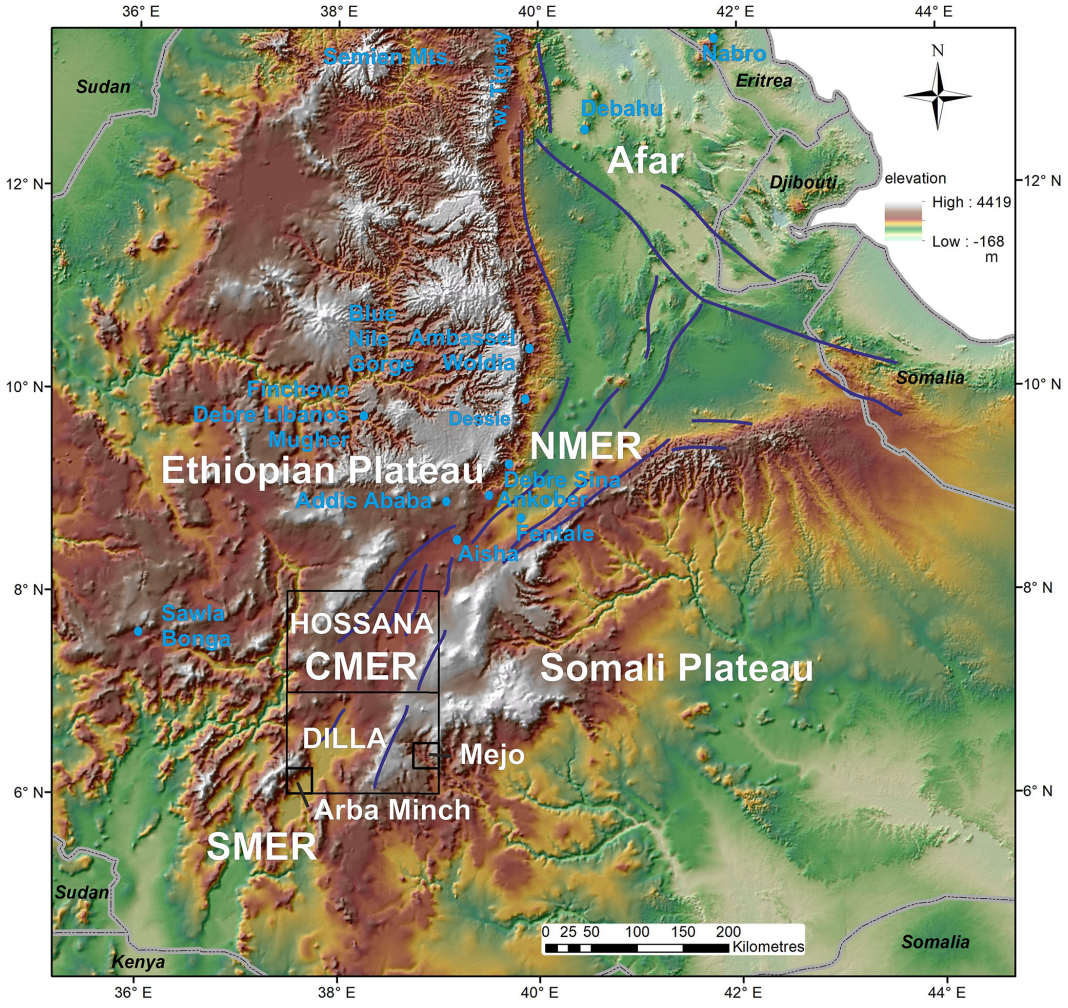

Figure 1. The Hossana and Dilla areas in the central and southern part of the Main Ethiopian Rift (MER). The location of the NMER (northern MER), CMER (central MER), SMER (southern MER), Mejo, and Arba Minch case study areas are also indicated. The blue lines represent major fault zones. Digital elevation models ASTER DEM and SRTM3, with a resolution of 30 m, were used (USGS EROS Archive; NASA LP DAAC).

prepared based on extensive and multiple types of field data to classify the lithological units into ranks of strength class as very low, low, medium, high, and very high rock mass strength units. These classifications are based on multiple criteria evaluations determined from field documentation, including intact rock strength, discontinuity conditions, and degree of weathering. The intact rock strength determination is made either by Schmidt hammers or testing representative irregular samples under the point load tester, and the results are normalized to the standard size of samples, as recommended by International Society for Rock Mechanics (ISRM, 1985) to IS_{50} reference strength. The discontinuity condition is determined by considering the spacing, aperture, and discontinuity surface roughness and overall geometry. The degree of weathering, on the other hand, is determined qualitatively on the bases of the criteria set out in British Standard (BS 5930; 1981) from various outcrops in the region.

3.2 Climatic data

The precipitation data were obtained from the national database that was set up by the Centre for Development and Environment (CDE), University of Bern, Switzerland in the 1990s for all of Ethiopia. Since the beginning, the data set has been upgraded with additional information layers, but the data set released as version I on a single CD-ROM, which has mean monthly precipitation data of the major settlement areas with information on the temporal coverage of recorded years, has been used in this study (Centre for Development and Environment, 1999). Precipitation point data (Centre for Development and Environment, 1999) were averaged (annual and for each month), and then the spatial distribution over the areas of interest were interpolated using the inverse distance weighted (IDW) method. Nevertheless, the precipitation seasonality index could not be calculated due to data

inhomogeneities, where only some stations have a recording period of more than 20 years but often less than 5 years. In order to calculate a seasonality index, 30 years continuity is required. Therefore, precipitation seasonality was evaluated using standard deviation among particular monthly precipitations and by wet (July and August) and dry season (December and January) differences. Monthly averages of all available data were considered for the calculations.

3.3 Remote sensing data and morphotectonic analysis

ASTER DEM (digital elevation model), SRTM3, and Landsat 7 ETM+ were used for morphotectonic analysis, the normalized difference vegetation index (NDVI) based on Modis (Terra Modis, U.S. Geological Survey (USGS) eMODIS Africa 10 d composite), and land use/land cover data available from the USGS (https://earthexplorer.usgs.gov/; last access: 15 October 2019; U.S. Geological Survey, 2017) were also evaluated. MODIS scenes from January (peak of dry season) and August (peak of wet season) 2016 were used for the vegetation assessment.

The main approach for the morphotectonic analysis followed that used by Dhont and Chorowicz (2006, and references therein). The main aim was to use DEM imagery to interpret the largest neotectonic structures in the central and southern MER regions. Single-directional and multidirectional shaded reliefs and an elevation-coloured ASTER DEM image (Fig. 3) was generated using ArcMap 10.6 (http://www.esri.com; last access: 5 November 2019). This DEM constitutes the basis for morphotectonic analysis at the regional scale. The faults mapped can be considered as being the main neotectonic faults because they have a prominent expression in the morphology. In some cases, they form asymmetric ranges, with one side corresponding to breaks in slope or scarps by the displacement of Pleistocene and Neogene lithological boundaries or by the occurrence of straight lines of kilometres to several tens of kilometres in length. The images were compared with field geological mapping data to distinguish the scarps formed by active faults from those formed by differential erosion of contrasted lithology.

The emplacement of volcanoes, which are abundant in study area, can also be related to tectonic structures such as tension fractures or open faults. Small volcanoes arranged along the straight lines or linear clusters of adjacent volcanoes were also interpreted as being linear structures. The result of the interpretation is called linear indices, which mostly represent active faults (normal and normal-oblique slip), but because of uncertainties in detailed lithology in some areas and a lack of field verification in some cases, the linear indices may also represent prominent fracture zones and, in exceptional cases, also lithological boundaries. To avoid such uncertainties, an independent evaluation of the geomorphology by numerical methods was carried out. For an evaluation of the main tectonic indications of the CMER and SMER, morphotectonic analysis was carried out at a regional scale of 1 : 250 000 (presented in Sect. 4.1 and 4.4), while case studies of Mejo and Arba Minch were evaluated on a detailed scale of 1 : 50 000 (Sect. 4.5). Linear indices are referred to as lineaments hereafter in the text and figures.

In addition to a visual interpretation of lineaments, a quantitative technique – morphometry – was also employed to analyse landforms in a quantitative manner. This technique uses numerical parameters such as slope, surface curvature, and convexity to extract morphological and hydrological objects (e.g. stream networks and landforms) from DEM (Fisher et al., 2004; Pike, 2000; Wood, 1996). Landforms and lithological units reflect also different geotechnical properties (e.g. rock strength and degree of weathering) so they can be identified by these numerical methods. Various studies have been carried out to link morphometry with fluvial erosion, tectonics and diverse geomorphological conditions, and volcanic activity (Altin and Altin, 2011; Bolongaro-Crevenna et al., 2005; Ganas et al., 2005; Kopačková et al., 2011; Rapprich et al., 2010). Morphometric maps were constructed utilizing Wood's algorithm based on Shuttle Radar Topography Mission (SRTM) DEM data (30 m pixel resolution). First, the topographic slope and the maximum and minimum convexity values were derived on a pixel-by-pixel basis. The variation in these parameters was quantified for each pixel with respect to neighbouring pixels (in orthogonal directions). Second, based on a set of tolerance rules, morphometric classes were defined for each pixel, i.e. ridge, channel, plane, peak, pit, and pass (Wood, 1996). Wood's (1996) algorithm allows the relief to be parameterized by setting different values for the tolerance of the topographic slope and convexity. In this study, the slope tolerance of 3.0 and convexity tolerance of 0.02 were used for the best fit.

4 Results and interpretations

The results of the regional study of morphotectonics, morphometric and field structural analysis, slope failure mapping, and a geostatistical evaluation of the relationships between tectonic, lithological, and surface conditions and the occurrence of the landslides are presented here. Also, a more detailed evaluation is finally carried out, taking two case study sites at the Mejo (on MER eastern shoulder) and Arba Minch (western MER escarpment) areas which have a contrasting geological and climatic setting across the MER.

4.1 Morphotectonic and morphometric analysis

Shaded relief maps, derived from DEMs with NW, N, and NE illumination, and multidirectional shaded relief maps were used as a base map for morphotectonic interpretation. After carrying out the first stage of a visual interpretation of the lineaments, the second stage was carried out on the automated/numerical morphology base map, which helped uncover some important lineaments with a not-so-prominent

morphological expression. Based on a comparison with geological maps, lineaments representing lithological boundaries, without the evidence of faults, were removed during the third stage. Thus, the interpreted lineaments mostly represent present-day active faults, fault zones, important fracture zones and, possibly, also shear zones (if there are any) which are manifested in morphology. Moreover, older faults with a prominent lithological contrast can be expressed in morphology. The interpretation was made on a scale of 1 : 250 000, so only the lineaments considered to represent a main fault or other tectonic zones have been mapped.

A combination of a visual morphotectonic interpretation, based on DEMs (Fig. 2) and an interpretation on morphometric landforms (Fig. 3), was used to map lineaments. The study area is characterized by a predominance of NNE–SSW-oriented lineaments mostly representing the major normal faults of the rift valley. The central and northern parts of the study area represent a relatively wider rift zone with extension spread over a larger area, while the southern part is narrower with steeper topographic gradients and more prominent vertical displacements on the faults. The subordinate population of lineaments, mostly perpendicular to the strike of the rift, has an E–W to WNW trend, while also showing vertical displacement.

4.2 Tectonics

The primary fabrics in rift-related volcanic deposits and lava flows are defined by the planar-preferred orientation of rock-forming minerals, micro-vesicles or micro-crystals and elongated mineral grains, lithic fragments, or stretched and welded pumice fragments. With the exception of the lateral parts of lava flows or volcanic centres, these planar fabrics are predominantly flat-lying or dip gently to ∼ SSW or E. In addition, a large amount of fault structures associated to the ∼ NNE–SSW trending MER dip predominantly steeply to ∼ ESE in the western part of the rift and to ∼ WNW along its eastern margin. The main ∼ NNE–SSW trending faults also form a prominent escarpment and other morphological features of the MER (Figs. 4a, 5). These faults are associated with fault lineation (slickensides) plunging steeply to moderately to ∼ SE (in the western escarpment) or to ∼ NW (in the eastern escarpment), both bearing exclusively normal kinematic indicators (Fig. 6a–c). There are two subordinate sets of fault structures that appear to be synchronous with the main ∼ NNE–SSW faults that are mostly perpendicular, WNW(W)–ESE(E) trending normal faults with predominantly NNW plunging slickensides, or steeply ∼ NNW dipping normal faults (Fig. 5a). Relatively younger or newly reactivated ∼ NNW(N)–SSE(S) trending faults which are oblique by ∼ 20–30° to the main fault system were mapped mainly in the central part of the rift valley (Figs. 2, 5a). In addition, ∼ NNW–ESE, ∼ NE-SW, and ∼ WSW–ENE trending strike-slip faults, with a gently prevailing right-lateral kinematic pattern, were identified across the studied area (Figs. 2, 5b). In the spatial context of large volcanic centres (e.g. Wobitcha, Duguna Fango, and Awassa caldera; Fig. 2) the caldera-related ring faults were found to have a curved asymmetric shape, mostly parallel to the caldera rim. These faults predominantly dip steeply to moderately inward to the centre of the caldera. Extensional joints occur in three distinct sets with a ∼ N–S, NNE–SSW, and E(WNW)–W(ESE) trend (Fig. 5c).

4.3 Areas prone to slope instabilities

The principal feature of the MER is the graben bounded by normal faults. The drainage network is largely controlled by tectonic activity and lithological variation. Parts of grabens form endorheic depressions are filled by temporal lakes. The area is climatically highly variable; the average amounts of annual rainfall vary from 500 mm in the Gibe and Omo gorges to 2600 mm on the escarpments and the adjacent highlands. The mean annual temperature is about 20 °C (Yekoye et al., 2012; Habtamu et al., 2012; Rapprich and Eshetu, 2014; Rapprich et al., 2014).

Slope failures, erosion, floods, and the occurrence of ground fissures are the most common geological hazards investigated in the Hossana and Dilla areas. Landslides, debris flows, and rockfalls represent common exogenous hazards distributed mainly on the fault scarps (Figs. 2 and 7a). The subsidence of the rift floor and consequent uplift of the highland lead to isostatic disequilibrium resulting in intensive headward erosion and slope processes. Most of the slope instabilities represent deep-seated complex fossil slumps or translational or rotational slides (Fig. 7b) that host reactivated smaller landslides and debris flows which are triggered by adverse anthropogenic practices (road construction, deforestation, and overgrazing) or river undercutting (Fig. 7e, f). The landslides develop in the succession of competent volcanic rocks – basalts and welded ignimbrites intercalated by highly weathered pyroclastics and horizons of palaeosoils – following the slip zone of these landslides. The steep slopes of the highly decomposed volcanic rocks due to columnar jointing are subject to toppling and rockfalls.

Rare lateral spread, with typical horst and graben features at the head, have been encountered in the complex unwelded ignimbrites and unconsolidated pyroclastic deposits, with horizons of palaeosoils following the slip zone of this landslide (Fig. 7c). Topographic depressions with a higher degree of saturation are often noted to have the long-term effect of triggering landslides and debris flow on the slopes below them (Fig. 7d, f). More detailed descriptions of slope instabilities in the Mejo and Arba Minch areas are given in Sect. 4.5 and in Figs. 9 and 11.

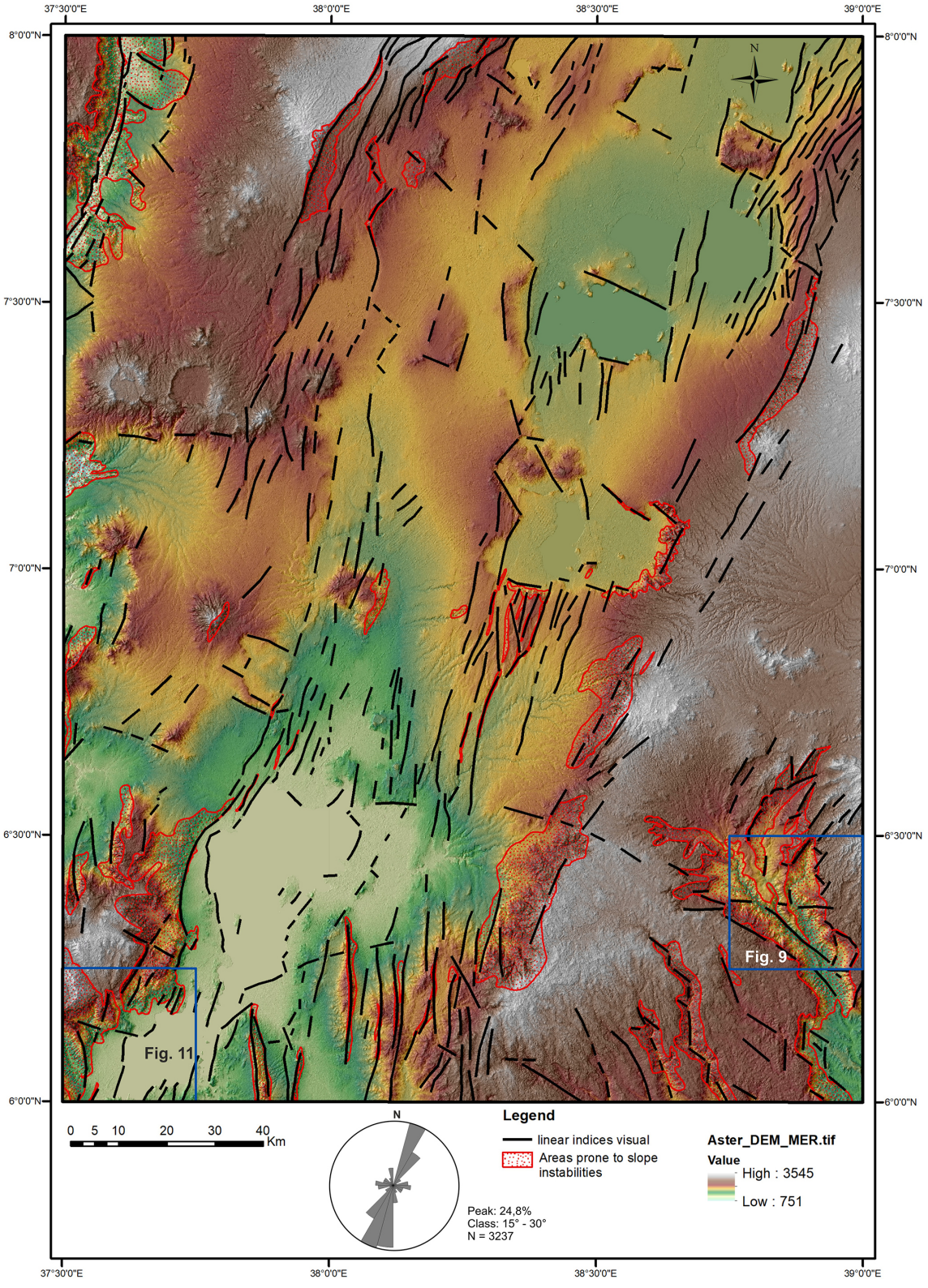

Figure 2. DEM (colour elevation map on multidirectional shaded relief) of the Dilla and Hossana areas, with visually interpreted linear indices and the distribution of their strikes in a rose diagram. The locations of the Mejo (Fig. 9) and Arba Minch (Fig. 11) detailed study areas are also shown (see Sect. 4.5). Digital elevation models ASTER DEM and SRTM3, with a resolution of 30 m, were used (USGS EROS Archive; NASA LP DAAC).

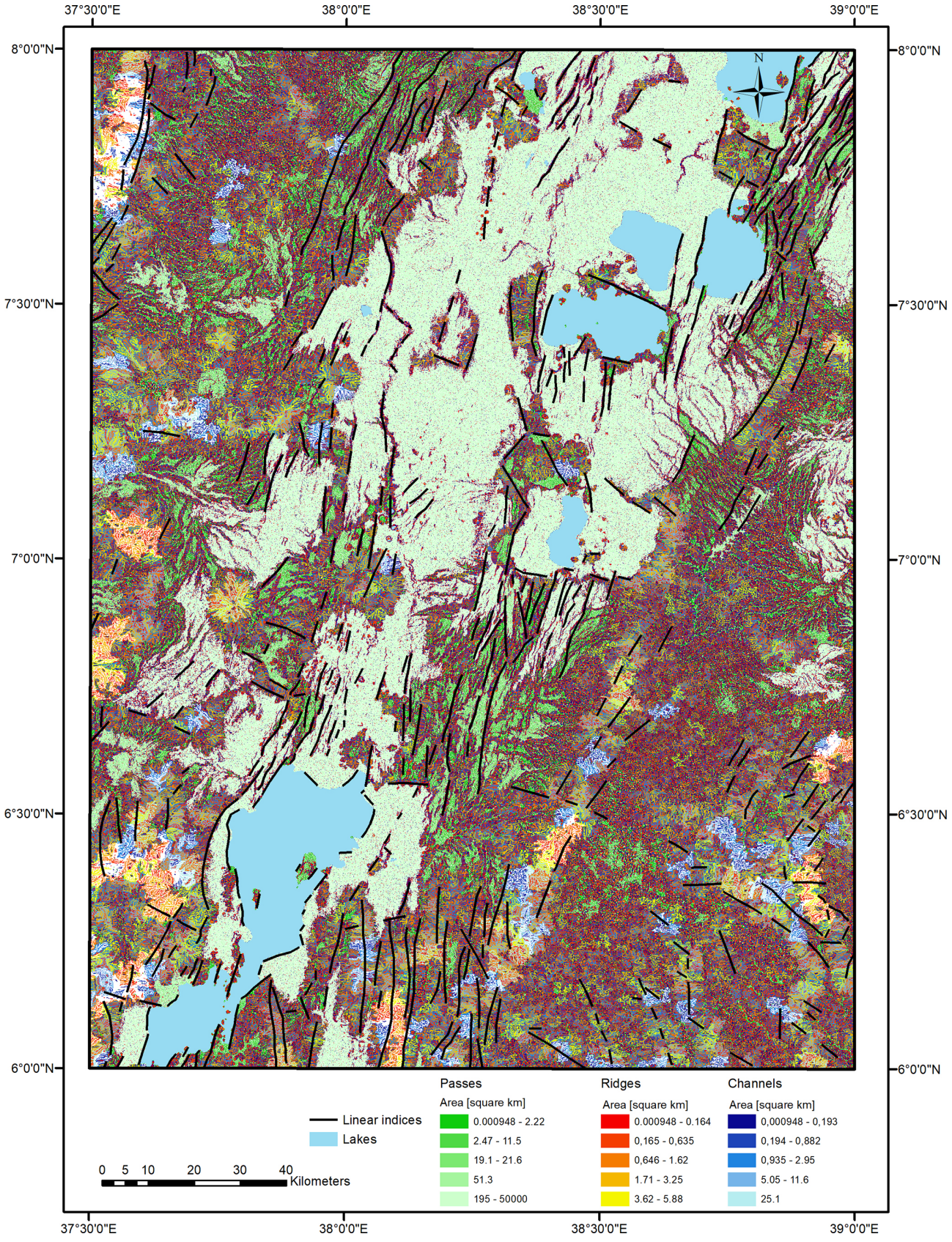

Figure 3. Morphotectonic analysis of the Dilla and Hossana areas based on morphometry. Linear indices show only the lines which are in accordance with both the visual interpretation of the DEM and the morphometry.

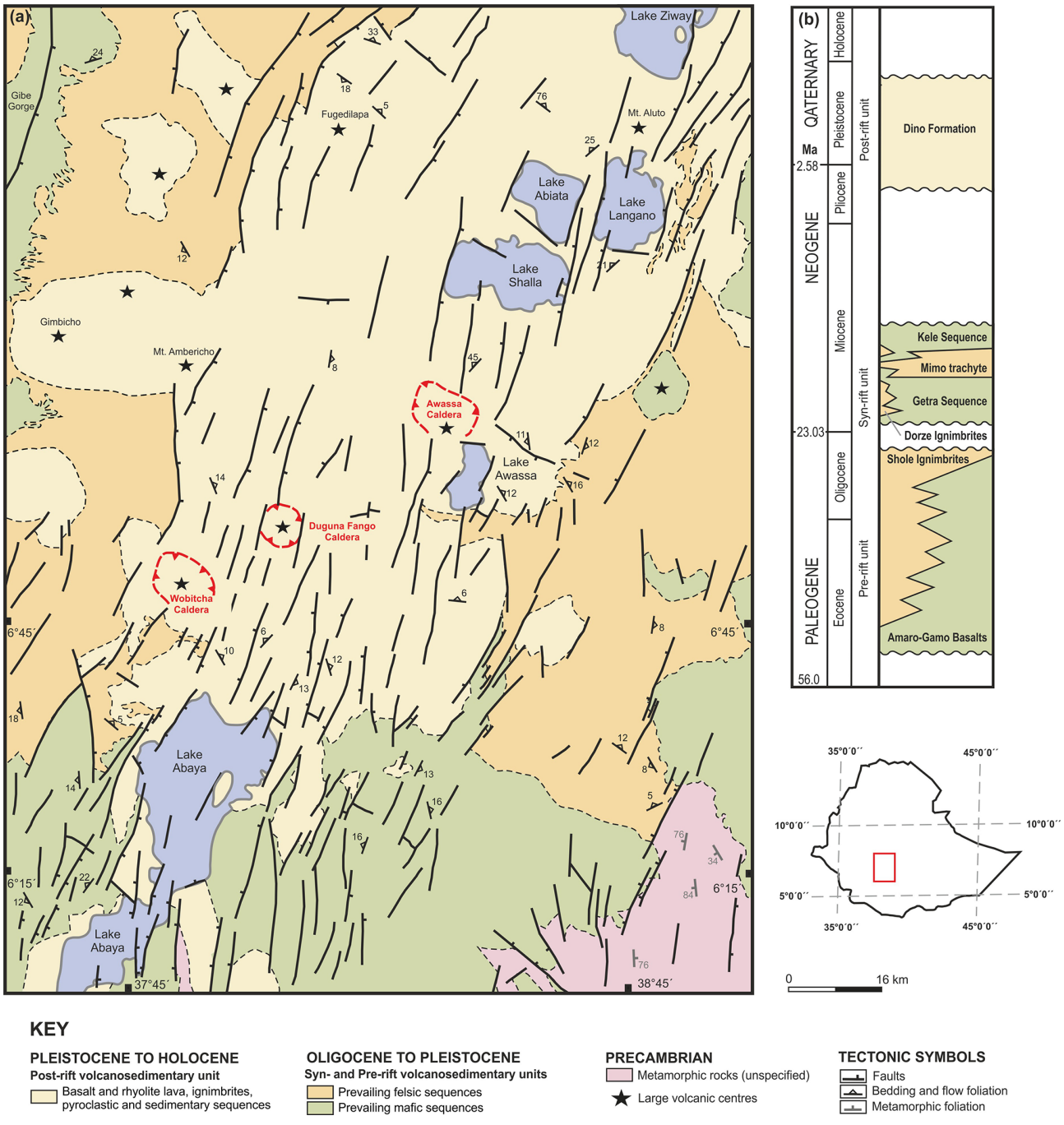

Figure 4. **(a)** Simplified geological map of the southern part of the Main Ethiopian Rift (Hossana and Dilla areas). **(b)** Schematic stratigraphic chart of the Main Ethiopian Rift (Dilla and Hossana areas). Compiled using unpublished geological maps (1 : 250 000; Geological Survey of Ethiopia).

4.4 Statistical analysis

Statistical analysis was carried out to better understand the influence of various surface processes and conditions (precipitation, vegetation, slope, and land cover) and geological parameters (rock mass strength, proximity of faults, and lineaments) on the formation of landslides and rockfalls. However, anthropogenic factors could not be evaluated statistically because the relevant data are not available. This section refers to regional mapping on a 1 : 250 000 scale, where areas prone to geohazards rather than particular geohazards were mapped. The results should be interpreted in this light.

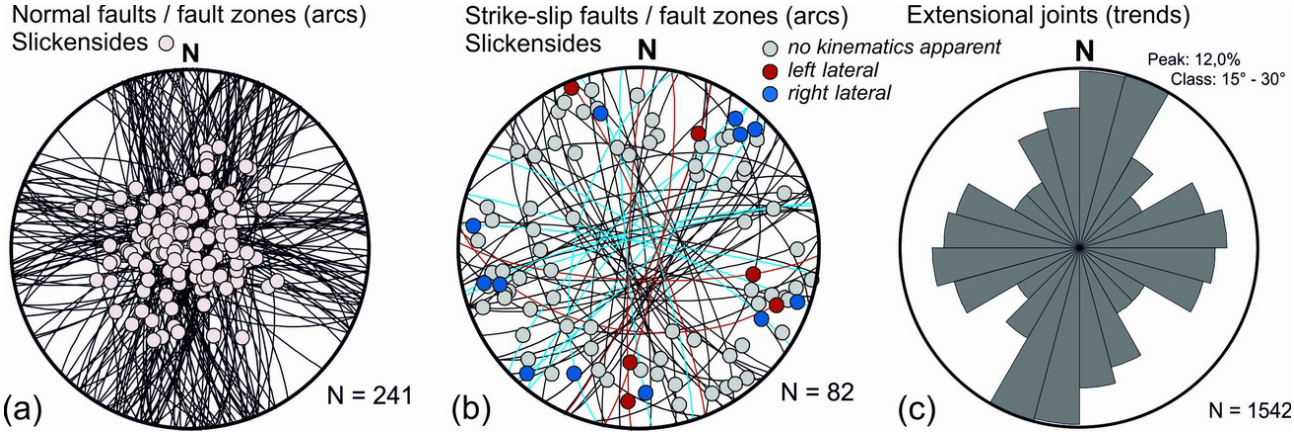

Figure 5. Field structural measurements of faults (equal area projection to the lower hemisphere) and extensional joints (rose diagram) from the southern part of the Main Ethiopian Rift (Hossana and Dilla areas).

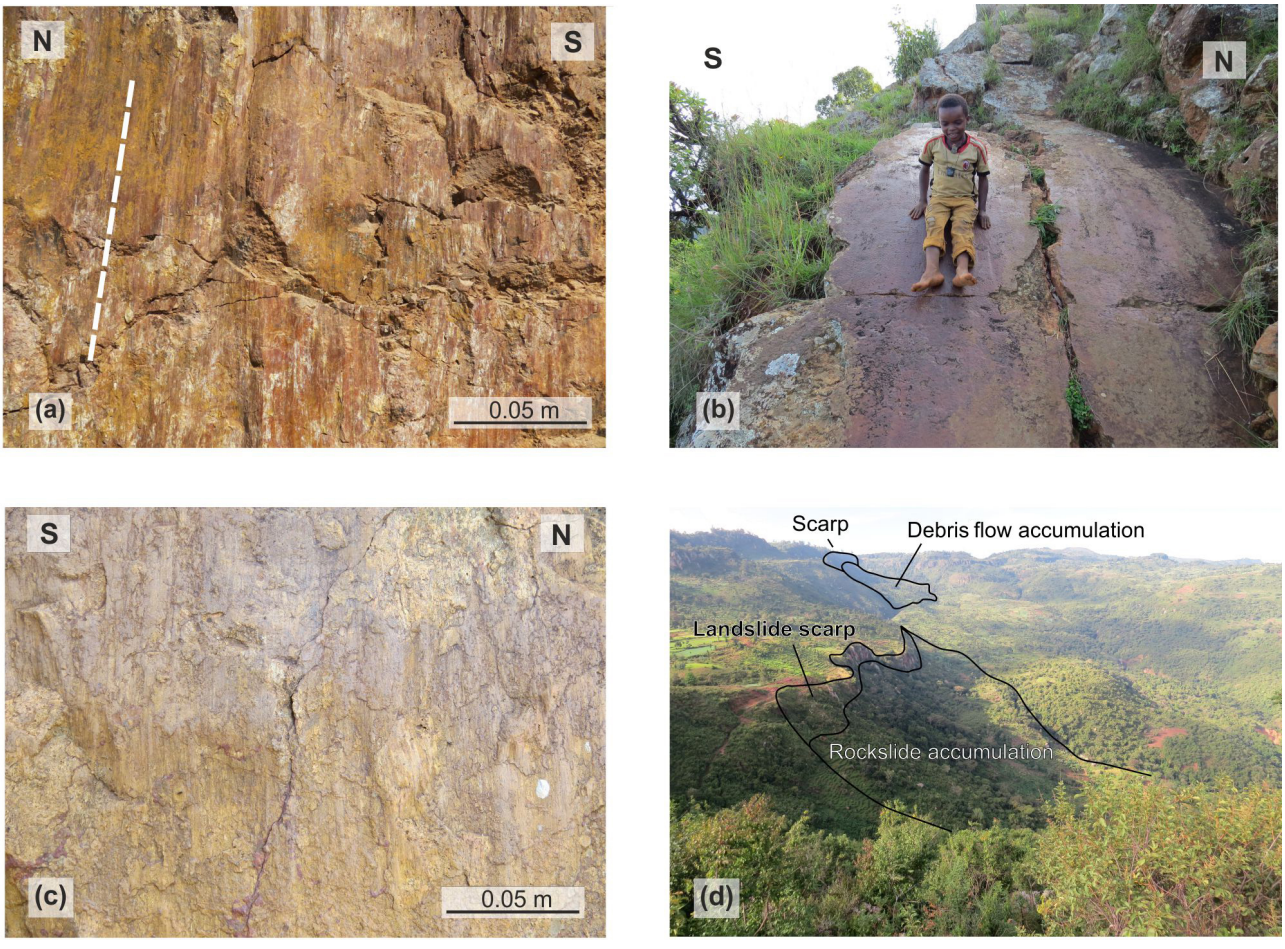

Figure 6. Field photographs. **(a)** Steeply dipping, N–S oriented fault plane, with steeply plunging slickensides and normal kinematic indicators (west of Dilla; eastern rift escarpment). **(b)** ESE moderately dipping normal fault, parallel with the main NNE–SSW trending western rift escarpment (Ocholo village; north of Arba Minch). **(c)** Steeply dipping, N–S oriented fault plane, with steeply plunging slickensides and normal kinematic indicators (Mejo plateau; ca. 60 km east of the main rift valley). **(d)** Rockslide and debris flow on normal fault slope north of Arba Minch.

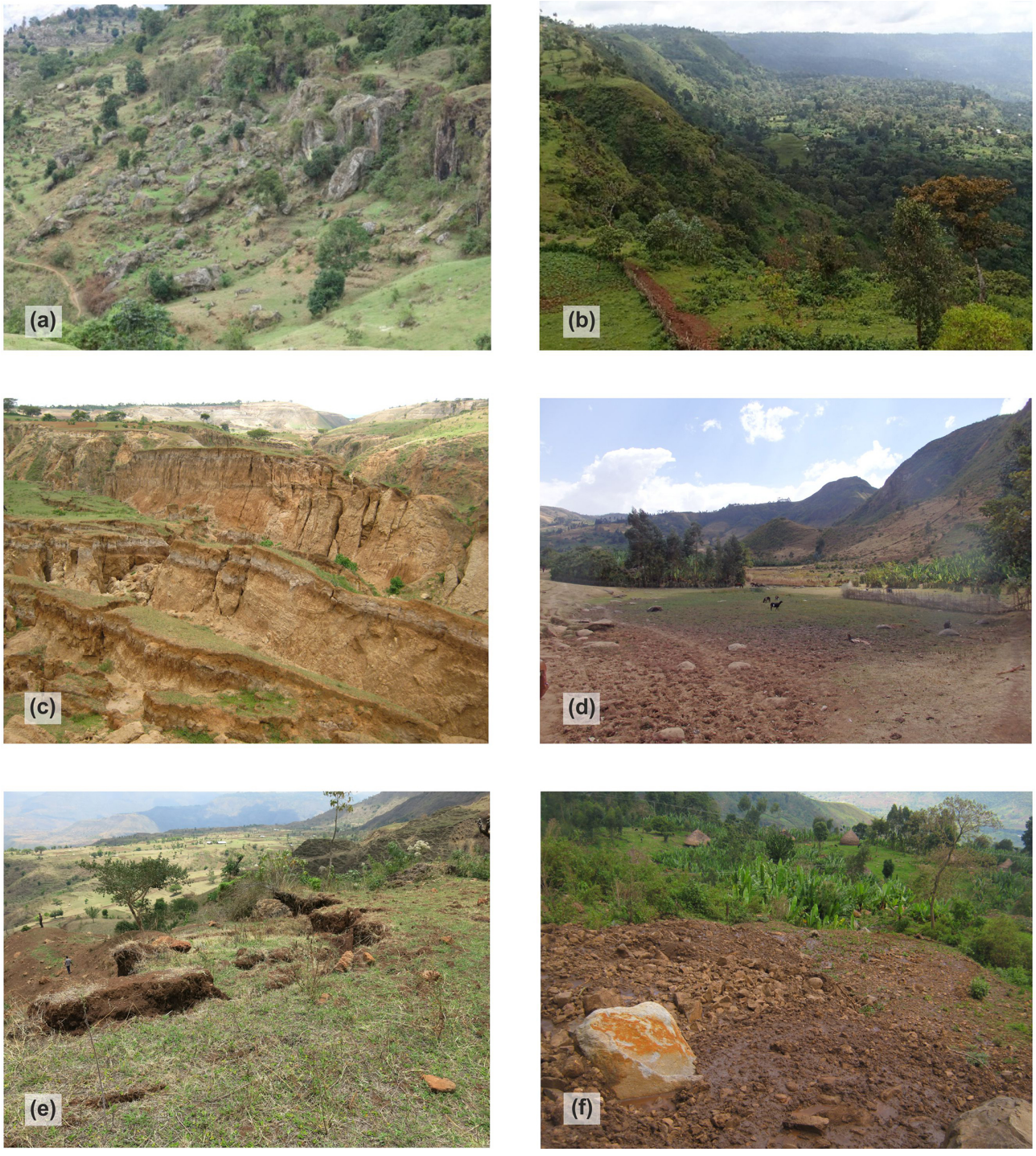

Figure 7. Field photographs of various types of geohazards in MER (Hossana and Dilla areas). **(a)** Toppling and subsequent rockfall of welded ignimbrites in the crown of a deep-seated landslide situated close to a fault scarp in the western highland area (Dilla area; NW of Arba Minch). **(b)** Large landslide in Dilla area (5 km SW of Mejo). **(c)** Tilted blocks of deep-seated landslide southwest of Awassa. **(d)** Undrained depression in the deep-seated fossil landslide east of Dilla. **(e)** Tension cracks in the crown of a shallow landslide reactivated by road construction (west of Arba Minch). **(f)** Recent debris flow accumulation below the road construction in the landslide area west of Mejo.

4.4.1 Descriptive statistics

For the purposes of descriptive statistics, the rock mass strength (RMS) was coded as follows: very high RMS (VHRMS) is equal to 7, high RMS (HRMS) is equal to 6, medium RMS (MRMS) is equal to 5, low RMS (LRMS) is equal to 4, very low RMS (LRMS) is equal to 3, soils are equal to 2, and lacustrine deposits are equal to 1. A significant correlation between RMS and slope and most precipitation parameters was found (see Table 1). More wet and seasonal areas occur on steeper slopes formed by stronger (less weathered) rocks. Most of the steep slopes in the study area are active normal fault escarpments. Another interesting statistically significant correlation is shown by slope, and most of the precipitation parameters and the NDVI of the dry period. Steeper slopes and higher altitudes attract clouds and precipitation, while flat lowlands allow clouds to pass by without precipitation. Significant correlations can also be found within various precipitation parameters, within selected vegetation parameters, and also between these two groups (precipitation and vegetation), which was supposed. No significant correlation was found between the proximity of faults and lineaments (expressed by faults and lineaments density) and other parameters. It seems to be an independent variable very suitable for further geostatistical evaluation. There is a high density of faults and lineaments in areas where faults and lineaments of different strikes cross; these areas do not necessarily have higher slopes. For other tectonic parameters, such as faults and lineament proximity, it is difficult to calculate by conventional correlation; hence, they are evaluated geostatistically in the following sections.

4.4.2 Geostatistics

The mean values of various geological, tectonic, climatic, vegetation, and land use factors were calculated for each landslide polygon area. The normalized difference vegetation index (NDVI) is adopted from MODIS images of 2016, while the density of lineaments is expressed as $\times 10^6$. The Kernel Density tool (under Spatial Analyst Tools/Density in ArcGIS 10.6) was used to evaluate the faults and lineaments density in MER on a scale of 1 : 250 000 (see Table 2). The proximity to tectonic features is expressed in terms of the percentage area of a particular geohazard within a particular buffer zone (500 m and 1 km buffer).

Most landslides and rockfalls form on steeper slopes close to faults and in areas with higher lineament density. Rockfalls are formed on steeper slopes than landslides (Table 2; see also see Figs. 2, 9, and 11), but slope factor has higher importance for the formation of landslides (in comparison to other factors; see Fig. 8). Rockfalls typically occur in areas receiving lower precipitation. Most of them occupy areas with grassland and, to a lesser extent, also on cultivated land and bush land cover. Higher vegetation seasonality is also found to coincide well with rockfall occurrences. There is a high vegetation difference between the dry season (January) and the rainy season (August; see Table 2). This is probably because fault escarpment vegetation, which grows in difficult conditions on steep rocky slopes, is more sensitive to precipitation seasonality. The low, very low, and high rock mass strength class probably influence the occurrence of rockfalls (see Table 2 and Fig. 8) but not medium rock mass strength. Probably because hard rocks are jointed, and then rockfalls with big blocks occur, these polygons also include slope deposits, classified as low to very low RMS, while landslides are formed in areas with higher precipitation and higher precipitation seasonality. Woodland, bushland, grassland, and cultivated areas with higher vegetation density and low vege-

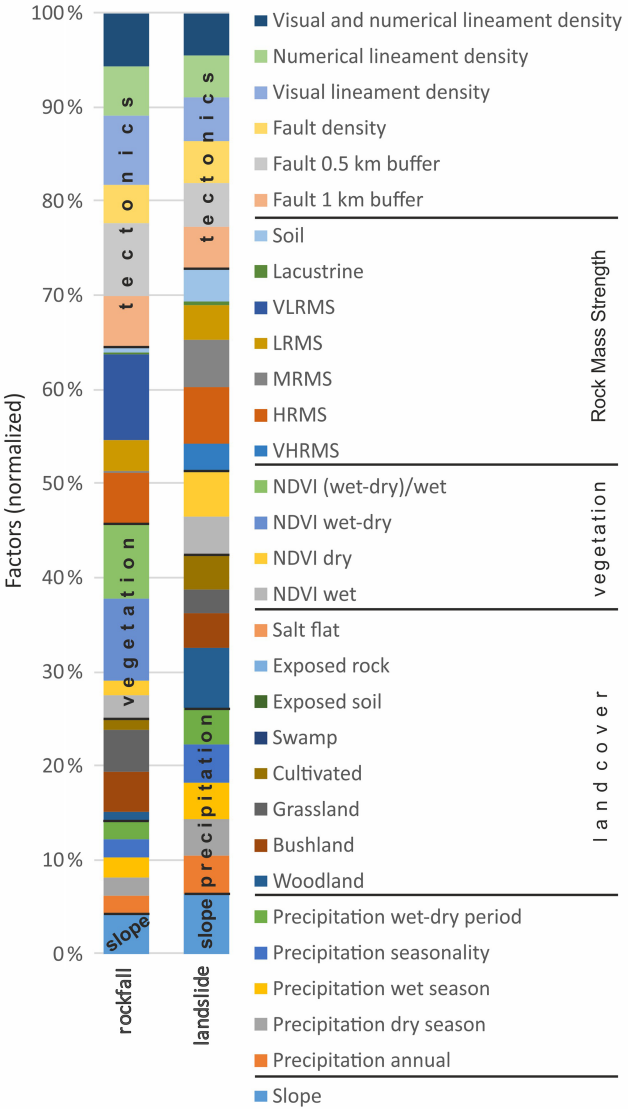

Figure 8. Plot of mean values of particular factors occurring across landslides and rockfalls polygons normalized to the mean value for the whole area. Diagram shows the relative importance of each factor.

Table 1. Correlation matrix of the selected factors controlling distribution of geohazards in the MER area. The number of samples is 153, and the critical value for correlation coefficient (R) at the 95 % significance level is 0.195. A statistically significant (95 %) R is in bold.

	RMS	Slope	Precipitation					NDVI			Faults and lineaments
			Annual	Dry period	Wet period	Seasonality	Wet–dry period	Wet period	Dry period	Wet–dry period	density
RMS	1.00	**0.44**	**0.49**	0.17	**0.43**	**0.58**	**0.39**	0.10	0.07	−0.01	0.13
Slope	0.44	1.00	**0.37**	0.11	**0.25**	**0.37**	**0.22**	0.16	**0.24**	−0.12	−0.11
Precipitation annual	0.49	0.37	1.00	**0.61**	**0.47**	**0.73**	**0.35**	**0.28**	**0.37**	−0.16	−0.14
Precipitation dry period	0.17	0.11	0.61	1.00	−0.11	−0.01	**−0.27**	0.14	**0.41**	**−0.29**	−0.18
Precipitation wet period	0.43	0.25	0.47	−0.11	1.00	**0.80**	**0.99**	0.15	**−0.39**	**0.44**	0.06
Precipitation seasonality	0.58	0.37	0.73	−0.01	0.80	1.00	**0.77**	**0.20**	0.06	0.07	0.03
Precipitation wet–dry period	0.39	0.22	0.35	−0.27	0.99	0.77	1.00	0.12	**−0.44**	**0.47**	0.09
NDVI wet period	0.10	0.16	0.28	0.14	0.15	0.20	0.12	1.00	0.16	**0.46**	−0.05
NDVI dry period	0.07	0.24	0.37	0.41	−0.39	0.06	−0.44	0.16	1.00	**−0.80**	−0.10
NDVI wet–dry period	−0.01	−0.12	−0.16	−0.29	0.44	0.07	0.47	0.46	−0.80	1.00	0.06
Faults and lineaments density	0.13	−0.11	−0.14	−0.18	0.06	0.03	0.09	−0.05	−0.10	0.06	1.00

tation seasonality are found to have an affinity with landslide occurrences. The entire range of rock mass strength classes (low, medium, and high) occur in areas of landslides.

4.5 Case studies – Mejo and Arba Minch areas

We selected two areas with contrasting lithological, tectonic, climatic, and vegetation settings and a similar size and morphology of landslides and rockfalls for a detailed study. The study areas correspond with 1 : 50 000 mapping (for the location of the map sheets, see Fig. 2).

4.5.1 Mejo site

Geological and climatic setting

The Mejo study area is located 60 km east of the main rift valley on the upland plateau of the southeastern flank of the MER. The Gambelto and Genale rivers draining the area southeast of Somalia form a typical morphology, with deeply incised N–S trending valleys in the central part and volcanic plateaus along the southwestern and eastern margin (Fig. 9). These volcanic plateaus attain an elevation slightly above 2000 m a.s.l. (above sea level) in the east and around 2100 m a.s.l. in the southwest. Neoproterozoic medium-grade metamorphic rocks crop out mainly in the deeper part of the valleys below the altitude of ca. 1900 m, and the deepest parts reach below 1000 m a.s.l. Thus, the area has a prominent topography with an altitude difference of more than 1000 m; the average slope in the area is more than 14°. The overlaying volcanic deposits are of the Eocene to Pleistocene age (Verner et al., 2018a, d). The local climate is humid, the annual precipitation is ∼ 1200 to ∼ 1550 mm (average 1393 mm) and highly seasonal, usually with two peaks corresponding to April–May and August–October, with more than 125 mm monthly average rainfall, while the rest of the months have a monthly average rainfall of slightly more than 40 mm. The difference between the average wet (July and August) and dry season (December and January) is 310 mm (Centre for Development and Environment, 1999). Vegetation cover is dense (NDVI values are almost double compared to the Arba Minch area) and moderately seasonal (see Table 3). Due to intense weathering, the area is dominated by rocks with low and medium mass strengths. The dominant land cover is woodland and bushland and cultivated areas form up to 25 % of the area.

The area is formed by the following two units: (i) a metamorphic basement consisting of foliated biotite orthogneiss with minor lenses of amphibolites outcropped in the lower parts of the slope and the bottom of valleys. The orthogneiss is moderately to strongly weathered, and the lenses of amphibolites have higher intact strength with a lower degree of weathering. The foliation of metamorphic rocks is often oriented downslope, parallel with the topography of the instable slopes. (ii) The volcanic complex overlying the metamorphic basement is formed by a roughly 500 m thick succession of basalt and trachybasalt massive lava flows and intercalations of palaeosols, fine basaltic scoria layers, and epiclastic deposits up to 2 m thick. The lava flows are moderately to strongly weathered with high fissured permeability, and the pyroclastic layers, palaeosols, and strongly weathered horizons with a high content of clay minerals may form semi-horizontal barriers for water movement resulting in higher plasticity and a reduction in permeability (Verner et al., 2018a, d).

Faults

Most of the fault structures were identified in the complex of metamorphic rocks without evidence of young reactivation. The youngest faults and fault zones belonging to the East African Rift System are rare and have no significant effect on the overall tectonic pattern of the area. These minor faults dip steeply to ∼ E or ∼ W, bearing well-developed steeply plunging slickensides and normal kinematics. The minor subordinate set of normal faults have a ∼ W (WNW) to E (ESE) trend. The fault displacement is relatively low

https://doi.org/10.5194/nhess-21-3465-2021

Table 3. Mean values for each geohazard polygon area compared to the overall area of Mejo and Arba Minch, respectively. Values that are in bold and underlined are highly above average, while bold values are above average.

Geohazard/factor		Precipitation				P. seasonality		Vegetation		V. seasonality		Rock mass strength						Tectonics				Land use					
		Slope (°)	Annual (mm)	Dec + Jan (dry) (mm)	Jul + Aug (wet) (mm)	Monthly (1)	Wet–dry (mm)	NDVI wet (Aug)	NDVI dry (Jan)	NDVI Aug–Jan	(Aug–Jan)/Aug (%)	VHRMS (%)	HRMS (%)	MRMS (%)	LRMS (%)	Lacustrine (%)	1 km buffer (%)	0.5 km buffer (%)	Faults density	Lineaments density	Woodland (%)	Bushland (%)	Grassland (%)	Cultivated (%)	Water (%)
Mejo	Landslide and debris flow	**17.6**	1335	46	346	75	300	**6303**	**7278**	**−975**	−0.15	2.06		**31.7**	**60.8**	5.4	50.9	27	33.8	**58**	**72**	3		**26**	
	Whole area	14.2	1393	47	357	78	310	5548	6421	−874	−0.16	7.89		**28.3**	**41.9**	**22**	61.5	36	33.6	34	**53**	**19**	3.1	**24.8**	
Arba	Landslide and rockfall	**14.9**	1070	60	188	45	128	**5361**	**6412**	**−1051**	−0.20			**42.7**	**56.7**	0.6	**97.1**	**68**	**67.0**	**78**		**30**		**70**	
Minch	Whole area	9.8	1068	59	189	46	130	3051	3909	−858	−0.28		3.01	**21.2**	**49.5**	**26**	68.8	44	43.6	51	1.14	**19.2**		**51.2**	**28.4**

Table 2. Mean values for each geohazard polygon area compared to the whole area of Hossana and Dilla. NDVI calculated from MODIS images (https://earthexplorer.usgs.gov/; last access: 20 June 2018; U.S. Geological Survey, 2017), and the lineaments density is $\times 10^6$. The proximity of tectonics is expressed in the percentage area of the particular geohazard within the buffer. Values that are in bold and underlined are highly above average, while bold values are above average, and values in italic are below average.

Geohazard/factor	Precipitation				P. seasonality		Vegetation		V. seasonality		Rock mass strength							Tectonics		Lineaments density				Land use						
	Slope (°)	Annual (mm)	Dec + Jan (dry) (mm)	Jul + Aug (wet) (mm)	Monthly (1)	Wet–dry (mm)	NDVI wet (Aug)	NDVI dry (Jan)	NDVI Aug–Jan	(Aug–Jan)/Aug (%)	VHRMS (%)	HRMS (%)	MRMS (%)	LRMS (%)	VLRMS (%)	Lacustrine (%)	Soil (%)	Within 1 km buffer	Within 0.5 km buffer	Faults	Visual	Numerical	Vis. and num.	Woodland (%)	Bushland (%)	Grassland (%)	Cultivated (%)	Swamp (%)	Exposed soil (%)	Water (%)
Rockfall	**17.2**	*1041*	44	312	54	268	**5412**	*3149*	**2263**	42	0	**27**	3	**40**	**25**	1	3	**88**	**66**	**155**	**341**	**227**	**227**	8	**18**	**48**	**21**	1	0	4
Landslide	**15.6**	**1248**	**51**	**351**	**66**	**300**	**5296**	**5510**	*-214*	−4	4	**18**	**38**	**26**	0	1	12	43	24	**97**	**131**	**111**	**108**	**38**	9	**16**	**37**	0	0	
Whole area	9.0	1172	48	333	61	285	4868	4297	571	12	5	11	28	26	6	11	13	36	19	82	103	95	88	22	9	24	36	1	1	6

across the area, reaching a maximum of 100 m in the vertical section (Verner et al., 2018a, d). The prominent morphology, with up to 1000 m deeply incised valleys, is made almost solely by erosion caused by the Neogene uplift.

Landslides and rockfalls

A large and deep-seated complex landslide area occurs in the slope of the eastern banks of the Gambelto valley. The landslide areas vary in length from several hundred metres to 4 km, with a width of up to 2 km (see Fig. 9). The landslide complexes are characterized by amphitheatre (horseshoe)-shaped edges of the main scarps and reach up to 200 m high and have 50 to 100 m high minor scarps. Commonly, tilted blocks, endorheic depressions, and a number of springs have also been noted in the landslide zone. Reactivated parts are characterized by small-scale (tens to hundreds of metres) and shallow-seated debris flows, slumps, and rockfalls accompanied by the subsidence of surface, cracks, or curved tree trunks, which were observed close to the new road construction.

Most landslides are fossil and inactive. The preservation of colluvial deposits is limited, while, in the depressed domain and the arched accumulation area of the landslide, they are covered by boulders and blocks. The morphology of the main and minor scarps is relatively sharp, and the accumulation zone is strongly modified by erosional processes with a smooth and undulating topography, an absence of a hummocky landscape and traverse ridges. Most of the reactivated parts are represented by small-scale and shallow-seated failures triggered by the poor design of local road construction.

Statistical evaluation

The mean values of the same factors as for the Hossana and Dilla areas (see Sect. 4.4.2) were also calculated for each landslide and rockfall polygon area in the case of the Mejo site. The same calculations and symbology as in Table 2 was used for most parameters, but faults and lineaments data were adopted from more detailed studies at a scale of 1 : 50 000 (Verner et al., 2018a, b, c, d), and the faults and lineaments density is calculated by a Line Density tool (ArcGIS 10.6.; Spatial Analyst Tools) and expressed as $\times 10^2$. Here the landslides and debris flows are situated in areas with much higher slopes compared to the overall study area (see Fig. 10 and Table 3). They are also formed in areas with a higher vegetation density and medium and low RMS. Landslide and debris flow areas have a much higher density of lineaments. They are also dominantly vegetated by woodlands, and cultivated areas are a minor land cover. Precipitation distribution does not show any significance; it can be due to the poor spatial resolution of the precipitation data. The same applies for the Arba Minch area.

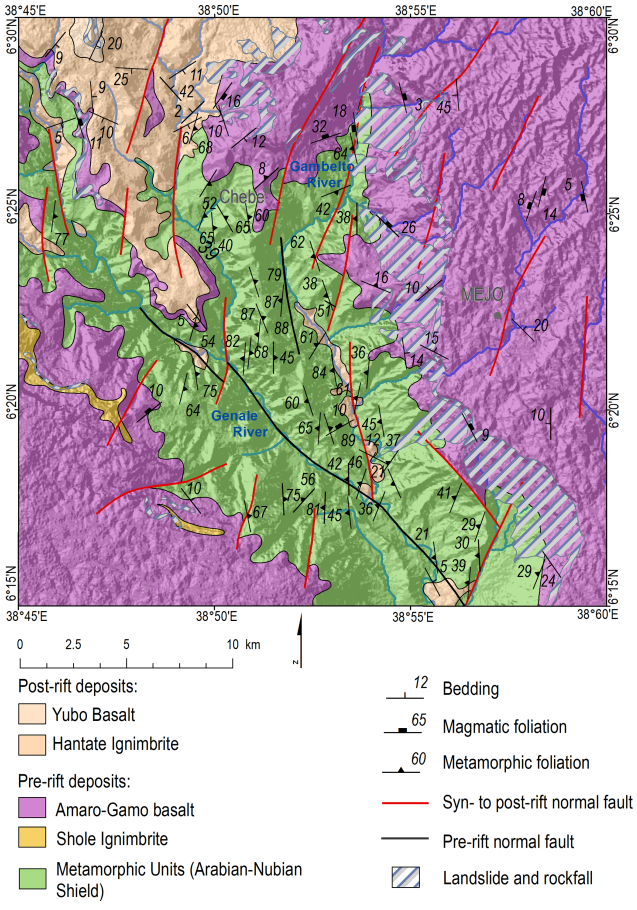

Figure 9. Geological and tectonic map of the Mejo site, with landslides and rockfalls indicated. For the location, see Fig. 2.

4.5.2 Arba Minch site

Geological and climatic setting

The Arba Minch study area is located directly in the main rift valley on the western normal fault escarpment. The total displacement of the syn- and post-rift normal faults is more than 1500 m. The average slope in the area is less than 10° because a large part of the area is covered by Abaya Lake (see Fig. 11). The area is less humid compared to Mejo, with an average annual precipitation of 1068 mm, and precipitation is moderately seasonal; the difference between the wet and dry season is 130 mm. But significant variations in precipitation have been recorded in apical parts of mountain ridges, such as Chencha, attaining, on average, an altitude of 2700 m a.s.l., with 1390 mm of rainfall, whereas, in the low-lying plains, with an average elevation of about 1200 m a.s.l. around the city of Arba Minch, the precipitation fluctuates around 780 mm (Centre for Development and Environment, 1999). Vegetation cover is moderate and moderately seasonal (see Table 3). Rocks with low and medium mass strengths and lacustrine deposits dominate the area. The dominant land

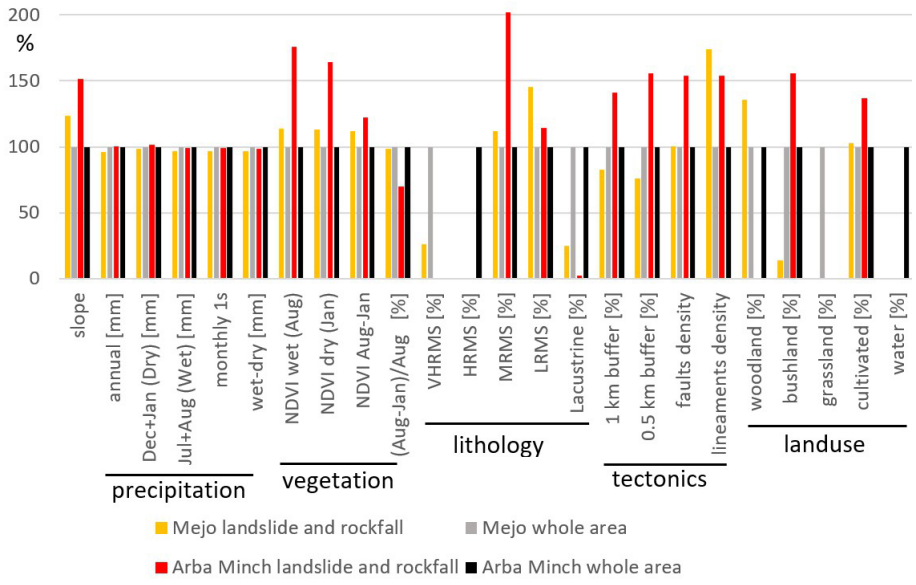

Figure 10. Plot of mean values of particular factors occurring across merged polygons of landslides and rockfalls normalized to the mean value for the overall area. Mejo and Arba Minch sites evaluated separately.

cover type is cultivated areas (from up to 51 %); bushland and water surface are also abundant types. The area is characterized by the lower Eocene to Pleistocene volcanic and volcaniclastic rocks, which are a product of episodic eruptions. They mostly have a bimodal composition, with alternating basic volcanic rocks and acidic pyroclastic rock intercalations (Verner et al., 2018b, c).

Faults

The prevailing faults are mostly parallel to the axis of the MER, forming the area's prominent morphological features. These major normal faults dip steeply to ESE or SE and trending NNE–SSE. Moreover, subordinate normal faults were identified, predominantly steeply inclined faults trending WNW–ESE, which are perpendicular to the prevailing rift parallel normal faults. Fault displacement is relatively high across the area, reaching a minimum of 1000 m, forming prominent morphology with an altitude difference of up to 1500 m between the plateau and graben floor.

Landslides and rockfalls

The slope failures are located in the western steep fault scarps separating the bottom of the rift valley with Abaya Lake, representing a local erosional base at an elevation of 1200 m a.s.l. and the western highland with an undulating landscape at an elevation of between 2000 and 2400 m a.s.l. The scarps are often modified by deep-seated slope failures. The lower parts of the slopes form moderately weathered basalts and trachybasalt, with minor pyroclastic fall layers of volcanic ash reaching up to 2 m in thickness and a reddish palaeosol up to 30 cm thick. The ridges and upper parts are formed from welded ignimbrites with minor rhyolitic ash fall deposits and palaeosol horizons. Volcanic rocks are variably affected by intense fracturing, jointing, and mega-tectonic fault systems. Basalts and trachybasalts are with a higher degree of weathering, while the welded ignimbrites with common columnar jointing are more resistant. The volcanic units have fissured permeability. Mainly the ignimbrites represent rocks with high permeability; on the other hand, the highly weathered basalt, the intercalation of fine grained pyroclastics, and palaeosol horizons could form hydrogeological horizontal barriers because of the high content of clay minerals. Most of the landslides are represented by deep-seated complex slope deformations including toppling, rockfall, rockslide, rotational landslides, and debris flows. These slope failures appear to be currently stable; the morphology is modified by subsequent exogenous processes as in the Mejo area. Only several small-scale active landslides triggered by river erosion and human intervention were observed.

Statistical evaluation

The mean values of the same factors as for the Mejo site were also calculated for each landslide and rockfall polygon area at the Arba Minch site. Here the landslides and rockfalls are situated in areas with much higher slopes compared to the overall study area (see Fig. 10 and Table 3). There is a much higher density of faults and lineaments close to faults. They are also formed in areas with much higher vegetation density and medium and low RMS. Landslide and rockfall areas are also dominantly covered by cultivated areas, with woodlands taking a minor role.

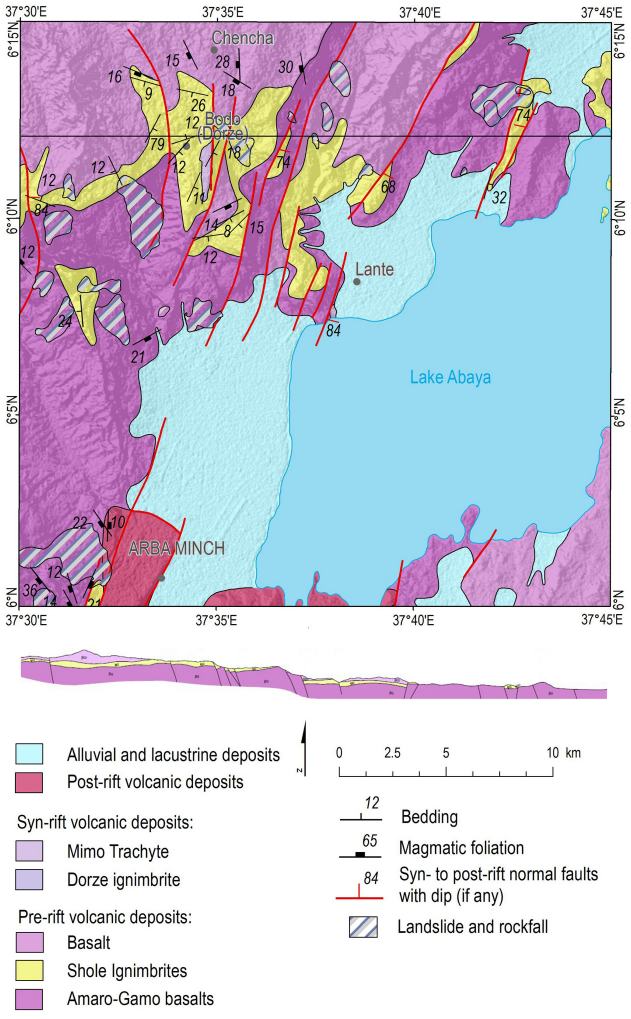

Figure 11. Geological and tectonic map of the Arba Minch site, with landslides and rockfalls indicated. For the location, see Fig. 2.

5 Discussion

The results discussed in the first subsection refer to regional mapping, where larger areas prone to geohazards rather than particular geohazards were mapped. Then, in the following subsections, there is a discussion of the detailed study of two areas (Arba Minch and Mejo) with contrasting lithological, tectonic, climatic, and vegetation settings and a similar size and morphology of landslides and rockfalls.

5.1 Main Ethiopian Rift (Hossana and Dilla area)

The progressive changes in the palaeostress regime during the active continental extension and faulting in the MER (e.g. Corti et al., 2018; Zwaan and Schreurs, 2020) increase the tectonic anisotropy of rocks and slope instabilities along major and subordinate fault escarpments, which have a pronounced effect on the genesis and formation of landslides. Several tectonic models explain the kinematics and palaeostress conditions of the regional extension/transtension from the beginning of the rifting (ca. 12 Ma) to the present (for the review, see Zwaan and Schreurs, 2020). Some models suppose continuous a NW–SE oriented extension (e.g. Chorowicz, 2005) in the early phase, which later changed to its current E–W direction (Bonini et al., 2005; Wolfenden et al., 2004). Alternatively, other models also assume a permanent E–W to ESE–WNW oriented extension (e.g. Agostini et al., 2009; Erbello and Kidane, 2018).

Proximity to faults and lineaments has a strong influence on the occurrence of areas prone to rockfalls and landslides in tectonically active areas worldwide (e.g. Chang et al,, 2018; Kumar et al., 2019, and references therein). According to statistical analysis, in the MER, both rockfalls and landslide areas typically occur on areas with steep slopes, close to faults and with a higher density of faults and lineaments. The latter parameter also reflects faults and fracture zone intersections and, according to geostatistic evaluation (Table 2), is more important for the formation of rockfalls than landslides. Rockfalls also show a much higher affinity to the proximity of faults. Most of them are normal faults associated with fissures opening during weathering, which initiates later rockfalls.

Rockfall areas occur in areas with lower precipitation, while, for landslides, high precipitation and high precipitation seasonality are typical. It correlates well with high vegetation density and low vegetation seasonality, which are found to have strong affinity with landslide occurrences. Thus, precipitation does not seem to be an important factor for rockfall formation but is important for landslides. It is probably because rockfalls are mapped on fault escarpments close to the rift valley, which is more dry, but they are initiated upslope at the edge of the plateau, where precipitation is higher.

Rockfalls and landslide areas occur in areas with bushland, grassland, and cultivated land cover. It leaves deforestation as one of the possible triggering factors. They also occur in areas with a wide range of rock mass strength classes (very low, low, medium, and high), so lithology and intensity of weathering do not seem to be an important triggering factor.

In the large area of the MER, the vast majority of slope instabilities is located on active normal fault escarpments (Fig. 12). This is a major natural triggering factor for rockfalls, while for landslides there is also the important influence of higher precipitation, precipitation seasonality, and vegetation density and vegetation seasonality.

5.2 Arba Minch case study

According to geostatistical analysis, the slope instabilities here, mostly landslides and rockfalls, are situated in areas with much steeper slopes, a much higher density of faults and lineaments, and are close to major faults. The majority of the large-scale slope instabilities of this area are strongly

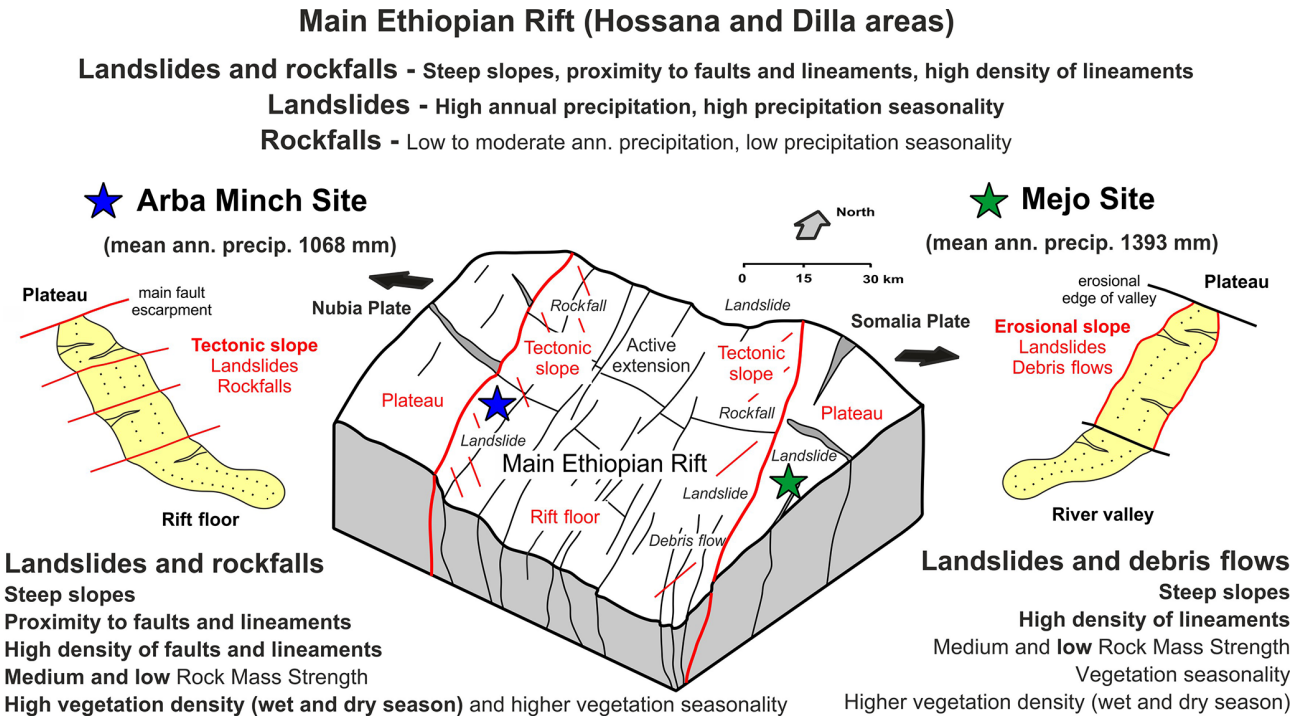

Figure 12. Sketch diagram summarizing the main factors controlling the formation and distribution of particular slope failures in the MER and in the Arba Minch and Mejo study sites.

associated with active tectonic morphological features characterized by straight fault scarps with triangular facets, large downthrown blocks, parallel sets of erosional valleys and asymmetrical ridges with SSW–NNE trending. These features are associated with active normal faults having large displacements (total vertical displacement of the western rift escarpment is more than 1500 m). Slope instabilities are also formed in areas with a much higher vegetation density and medium and low RMS. Volcanic rocks are variably affected by intense fracturing along faults; these zones are often altered, which lowers the slope stability of the rock environment. Alteration is also enhanced by more intense water–rock interactions – most springs are located on fault zones (Arba Minch means "forty springs"). Precipitation was not confirmed as an important factor.

The Arba Minch area is seismically active. According to the catalogue of earthquakes of the United States Geological Survey (USGS), several earthquakes have been documented around Abaya Lake since 1973 with magnitudes between 4 and 6 (U.S. Geological Survey, Earthquake Hazards Program, 2017). This active tectonic is also documented by young faults affecting Quaternary volcanic rocks and sediments outcropped around the town of Arba Minch (Verner et al., 2018b, c).

5.3 Mejo case study

Geostatistical analysis revealed that landslides and debris flows here are situated in areas with steep slopes. The geomorphology of the area is almost unaffected by local faults parallel with the rift valley; evidence of young faulting as displacement of the Pleistocene and Holocene rocks and straight fault scarps with triangular facets has not been observed. The steep slopes are formed and strongly modified by an intensive headward erosion. The incision of the valley as a result of a lowered erosional level and highland uplift could be the driving factor for the slope instability in the case of the Mejo area. Geomorphic proxies and the thickness of flood basalts suggest that the more tectonically active southeastern escarpment of the CMER and SMER (where the Mejo site is situated) are experiencing a relatively higher rate of tectonic uplift compared to the southeastern escarpment of the northern MER and the Afar Triangle (Xue et al., 2018; Sembroni et al., 2016). This can also be noted from the Eocene–Oligocene–Miocene basalts base (35–26 My) occurring in Arba Minch at an elevation of around 1050 m a.s.l., compared to their occurrence at a much higher elevation in Mejo at around 1900 m a.s.l. (Verner et al., 2018a, b, c, d).

Another factor causing the decrease in slope stability could be the following local lithological properties (dominance of medium and low RMS characteristic for slope instabilities in the area): (i) frequent intercalations of palaeosols with a high content of clay minerals and low permeability, or (ii) a

strongly weathered metamorphic basement with foliation often concordant with the landscape, forming a very weak lithological environment, which is favourable for slope processes. No young volcanic features and products have been observed; the probability of earthquakes related to volcanic eruptions is very low in the Mejo area, where the nearest earthquakes were recorded 60 km NW of the study area.

5.4 Comparison of the Arba Minch and Mejo sites

Landslides at both sites are similar from a geomorphological point of view, i.e. old, stabilized, and smoothed by erosion. The estimated age of landslides is Plio-Pleistocene, maybe even older, and uplift dates minimally last several megaannums (Ma), i.e. approximately the same interval plus the Holocene, so, in both cases, it concerns long-term evolution. Young reactivations are very localized and mostly due to human activity. Both study areas have seasonal humid climates with a prominent summer (mid-June to mid-September) rain season, but the Mejo study area, which is situated 90 km east of Arba Minch, 60 km out of the main rift valley on the uplifting plateau, is more humid. In the Mejo area. the mean annual rainfall is 30 % higher (1393 mm) compared to Arba Minch (1068 mm); most of the precipitation difference falls in the rainy season, while, during the dry months, the precipitation at both localities is comparable (Table 3).

Steep slopes associated with active faulting and hydrogeological conditions favouring rock alterations along these zones are probably the main predisposition for the formation of slope instabilities in Arba Minch. Seasonal precipitation and seismic events could be triggering factors.

The combination of a deeply weathered Proterozoic basement and steep slopes formed by intense headward erosional processes due to relatively rapid uplift could represent the main predisposition for creating favourable conditions for landslide evolution in Mejo (Fig. 12). Triggers of slope instabilities are probably more intense precipitation and higher precipitation seasonality.

6 Conclusions

Active continental rifting has a distinct effect on the formation of landslides. The formation, superposition, and polyphase reactivation of fault structures in the changing regional stress field increase the tectonic anisotropy of rocks and increase the risk of slope instabilities forming. The new structural data from the CMER and SMER support a model of progressive change in the orientation of the regional extension from NW–SE to the recent E(ENE)–W(WSW) direction driven by the African and Somali plates moving apart, with the presumable contribution of the NNE(NE)–SSW(SE) extension controlled by the Arabian Plate.

An evaluation at the regional scale of the central and southern MER demonstrates that areas prone to slope instabilities, mainly landslides and rockfalls, occur on steep slopes, which were almost exclusively formed on active normal fault escarpments. Landslide areas are also significantly influenced by higher annual precipitation, higher precipitation seasonality, and vegetation density and seasonality, while rockfalls have an affinity to vegetation seasonality only. Landslide areas occur on slopes at higher altitudes with higher precipitation and vegetation density, but large parts of the study area are on the rift floor, which is more dry, scarcely vegetated, very flat, and without landslides, while dense vegetation cannot develop on rockfalls occupying very steep rocky and blocky fault escarpments. Deforestation is also an important predisposition because rockfalls and landslides typically occur in areas with bushland, grassland, and cultivated land cover.

Different geological, geomorphological, and climatic conditions can lead to the formation of similar types of slope instabilities. A detailed study on active rift escarpment in the Arba Minch area revealed similar affinities as in the regional study of MER. Slope instabilities here are closely associated with steep, mostly faulted, slopes and a higher density of vegetation. Active faulting, forming steep slopes, is the main predisposition for landslide formation here, and the main triggers could be seismicity and seasonal precipitation.

While the detailed study situated in the Mejo area on the uplifting Ethiopian Plateau 60 km east of the rift valley shows that the occurrence of slope instabilities is strongly influenced by steep erosional slopes and the deeply weathered Proterozoic metamorphic basement, landslides here are often formed in areas densely fractured and with foliation concordant with topography. Regional uplift, accompanied by rapid headward erosion forming steep slopes together with unfavourable lithological conditions, is the main predisposition for landslide formation; the main triggers can be intense precipitation and higher precipitation seasonality. Triggers for young landslides are also very probably human activity and erosion, but the relevant data are lacking for a thorough evaluation and only occasional observations support this conclusion.

Data availability. Data are available upon request from the corresponding author.

Author contributions. KM prepared the paper, with contributions from all co-authors, and performed morphotectonic study, remote sensing data processing and analysis, statistic and geostatistical analysis and part of the field geological mapping. KV was responsible for the structural analysis and part of the field geological mapping. TH performed the geohazard mapping and analysis. LAM contributed with climatic and engineering geology data and did part of the field geohazard mapping. VK performed morphometric analysis. DB carried out part of the field geological mapping and provided information on rock lithologies. AM contributed to structural

analysis, RK helped with the preparation of the paper, and MY (with MK) did important parts of the field mapping.

Competing interests. The authors declare that they have no conflict of interest.

Disclaimer. Publisher's note: Copernicus Publications remains neutral with regard to jurisdictional claims in published maps and institutional affiliations.

Acknowledgements. We thank our many colleagues from the Geological Survey of Ethiopia and Addis Ababa University (School of Earth Sciences), for their help in the acquisition, processing and interpretation of the data, and especially Aberash Mosisa and Wubayehu Dessalegn Sallile. Many thanks to Richard Withers, for the English proofreading. The paper was enhanced by valuable comments from the editor, Filippo Catani, and two anonymous referees.

Financial support. The research has been funded by the Czech Development Agency in the framework of a development project (project no. 281226/2018-Č RA – "Implementation of a Methodical Approach in Geological Sciences to Enhance the Quality of Doctoral Studies at the Addis Ababa University (Ethiopia)" – and project 15 no. 280614/2019-Č RA – "Ensuring Sustainable Land-Management in Selected Areas of Ethiopia on the Basis of Geoscientific Mapping" – with both grants being awarded to Kryštof Verner) and project Q45 Progress (Faculty of Science, Charles University, Prague).

Review statement. This paper was edited by Filippo Catani and reviewed by two anonymous referees.

References

Abate, M., Nyssen, J., Steenhuis, T. S., Moges, M. M., Tilahun, S. A., Enku, T., and Adgo, E.: Morphological changes of Gumara River channel over 50 years, upper Blue Nile basin, Ethiopia, J. Hydrol., 525, 152–164, https://doi.org/10.1016/j.jhydrol.2015.03.044, 2015.

Abebe, T., Manetti, P., Bonini, M., Corti, G., Innocenti, F., Mazzarini, F., and Pecskay, Z.: Geological map (scale 1 : 200 000) of the northern main Ethiopian rift and its implication for the volcano-tectonic evolution of the rift, Geological Society of America, Boulder, Colorado, Maps and Charts series, MCH094, 2005.

Abebe, B., Dramis, F., Fubelli, G., Umer, M., and Asrat, A.: Landslides in the Ethiopian highlands and the Rift margins, J. Afr. Earth Sci., 56, 131–138, https://doi.org/10.1016/j.jafrearsci.2009.06.006, 2010.

Acocella, V.: Coupling volcanism and tectonics along divergent plate boundaries: Collapsed rifts from central Afar, Ethiopia, Geol. Soc. Am. B., 122, 1717–1728, https://doi.org/10.1130/B30105.1, 2010.

Agostini, A., Corti, G., Zeoli, A., and Mulugeta, G.: Evolution, pattern, and partitioning of deformation during oblique continental rifting: Inferences from lithospheric-scale centrifuge models, Geochem. Geophys. Geosyst., 10, 1–11, https://doi.org/10.1029/2009GC002676, 2009.

Agostini, A., Bonini, M., Corti, G., Sani, F., and Manetti, P.: Distribution of Quaternary deformation in the central Main Ethiopian Rift, East Africa, Tectonics, 30, 4010, https://doi.org/10.1029/2010TC002833, 2011.

Altin, T. B. and Altin, B. N.: Development and morphometry of drainage network in volcanic terrain, Central Anatolia, Turkey, Geomorphology, 125, 485–503, https://doi.org/10.1016/j.geomorph.2010.09.023, 2011.

Asfaw, L. M.: Development of earthquake-induced fissures in the Main Ethiopian Rift, Nature, 297, 393–395, https://doi.org/10.1038/297393a0, 1982.

Asfaw, L. M.: Seismic risk at a site in the East African rift system, Tectonophysics, 209, 301–309, https://doi.org/10.1016/0040-1951(92)90038-8, 1992.

Asfaw, L. M.: Environmental hazard from fissures in the Main Ethiopian Rift, J. Afr. Earth Sci., 27, 481–490, https://doi.org/10.1016/S0899-5362(98)00074-8, 1998.

Asfaw, L. M.: Integrated approach to the study of geohazards with application in southern Afar, J. Afr. Earth Sci., 48, 237–244, https://doi.org/10.1016/j.jafrearsci.2006.08.006, 2007.

Ayalew, L.: The effect of seasonal rainfall on landslides in the highlands of Ethiopia, B. Eng. Geol. Environ., 58, 9–19, https://doi.org/10.1007/s100640050065, 1999.

Ayalew, L. and Yamagishi, H.: Slope failures in the Blue Nile basin, as seen from landscape evolution perspective, Geomorphology, 57, 95–116, https://doi.org/10.1016/S0169-555X(03)00085-0, 2004.

Ayalew, L., Yamagishi, H., and Reik, G.: Ground cracks in Ethiopian Rift Valley: facts and uncertainties, Eng. Geol., 75, 309–324, https://doi.org/10.1016/j.enggeo.2004.06.018, 2004.

Ayele, A.: Probabilistic seismic hazard analysis (PSHA) for Ethiopia and the neighboring region, J. Afr. Earth Sci., 134, 257–264, https://doi.org/10.1016/j.jafrearsci.2017.06.016, 2017.

Ayele, A., Jacques, E., Kassim, M., Kidane, T., Omar, A., Tait, S., Nercessian, A., de Chabalier, J. B., and King, G.: The volcano–seismic crisis in Afar, Ethiopia, starting September 2005, Earth Planet. Sc. Lett., 255, 177–187, https://doi.org/10.1016/j.epsl.2006.12.014, 2007.

Ayele, A., Keir, D., Ebinger, C., Wright, T. J., Stuart, G. W., Buck, W. R., Jacques, E., Ogubazghi, G., and Sholan, J.: September 2005 mega-dike emplacement in the Manda-Harraro nascent oceanic rift (Afar Depression), Geophys. Res. Lett., 36, L20306, https://doi.org/10.1029/2009GL039605, 2009.

Ayenew, T. and Barbieri, G.: Inventory of landslides and susceptibility mapping in the Dessie area, northern Ethiopia, Eng. Geol., 77, 1–15, https://doi.org/10.1016/j.enggeo.2004.07.002, 2005.

Billi, P.: Geomorphological landscapes of Ethiopia, in: Landscapes and Landforms of Ethiopia, Springer, Dordrecht, 3–32 pp., https://doi.org/10.1007/978-94-017-8026-1_1, 2015.

Billi, P. and Dramis, F.: Geomorphological investigation on gully erosion in the Rift Valley and the northern highlands of

Ethiopia, Catena, 50, 353–368, https://doi.org/10.1016/S0341-8162(02)00131-5, 2003.

Bolongaro-Crevenna, A., Torres-Rodríguez, V., Sorani, V., Frame, D., and Ortiz, M. A.: Geomorphometric analysis for characterizing landforms in Morelos State, Mexico, Geomorphology, 67, 407–422, https://doi.org/10.1016/j.geomorph.2004.11.007, 2005.

Bonini, M., Corti, G., Innocenti, F., Manetti, P., Mazzarini, F., Abebe, T., and Pecskay, Z.: Evolution of the Main Ethiopian Rift in the frame of Afar and Kenya rifts propagation, Tectonics, 24, 1–24, https://doi.org/10.1029/2004TC001680, 2005.

British Standard BS5930: Code of Practice for Site Investigations, British Standards Institution (BSI), London, 147 pp., 1981.

Burianek, D., Hroch, T., Verner, K., Megerssa, L., Martinek, K., Yakob, M., Haregot, A., Janderkova, J., Sima, J., Krystofova, E., Valenta, J., Tadesse, E., Mosisa, A., Dalke, G., Legesse, F., Assefa, G., Pecskay, Z., Hejtmankova, P., and Krejci, Z.: Explanatory notes to thematic geoscientific maps of Ethiopia at a scale of 1 : 50 000, Map Sheet 0638-C2 Dila, Czech Geological Survey, Prague, 103 pp., 2018.

Centre for Development and Environment: Ethio GIS CD-ROM Database file system, University of Bern, Switzerland, 1999.

Chang, K.-J., Chan, Y.-C., Chen, R.-F., and Hsieh, Y.-C.: Geomorphological evolution of landslides near an active normal fault in northern Taiwan, as revealed by lidar and unmanned aircraft system data, Nat. Hazards Earth Syst. Sci., 18, 709–727, https://doi.org/10.5194/nhess-18-709-2018, 2018.

Chorowicz, J.: The east African rift system, J. Afr. Earth Sci., 43, 379–410, https://doi.org/10.1016/j.jafrearsci.2005.07.019, 2005.

Corti, G.: Continental rift evolution: From rift initiation to incipient break-up in the Main Ethiopian Rift, East Africa, Earth-Sci. Rev., 96, 1–53, https://doi.org/10.1016/j.earscirev.2009.06.005, 2009.

Dhont, D. and Chorowicz, J.: Review of the neotectonics of the Eastern Turkish–Armenian Plateau by geomorphic analysis of digital elevation model imagery, Int. J. Earth Sci., 95, 34–49, https://doi.org/10.1007/s00531-005-0020-3, 2006.

Ebinger, C. J., Yemane, T., Woldegabriel, G., Aronson, J. L., and Walter, R. C.: Late Eocene-Recent volcanism and faulting in the southern Main Ethiopian Rift, J. Geol. Soc., 150, 99–108, https://doi.org/10.1144/gsjgs.150.1.0099, 1993.

Ebinger, C. J., Yemane, T., Harding, D. J., Tesfaye, S., Kelley S., and Rex D. C.: Rift deflection,migration, and propagation: Linkage of the Ethiopian and Eastern rifts, Africa, Geol. Soc. Am. B., 112, 163–176, https://doi.org/10.1130/0016-7606(2000)112<163:RDMAPL>2.0.CO;2, 2000.

Erbello, A. and Kidane, T.: Timing of volcanism and initiation of rifting in the Omo-Turkana depression, southwest Ethiopia: Evidence from paleomagnetism, J. Afr. Earth Sci., 139, 319–329, https://doi.org/10.1016/j.jafrearsci.2017.12.031, 2018.

FAO, Food and Agriculture Organization: Global Forest Resources Assessment 2000: Main Report, FAO Forestry Paper 140, Rome, Italy, https://doi.org/10.1016/S0264-8377(03)00003-6, 2001.

Fisher, P., Wood, J., and Cheng, T.: Where is Helvellyn? Fuzziness of multi-scale landscape morphometry, Transactions of the Institute of British Geographers, 29, 106–128, https://doi.org/10.1111/j.0020-2754.2004.00117.x, 2004.

Fritz, H., Abdelsalam, M., Ali, K. A., Bingen, B., Collins, A. S., Fowler, A. R., Ghebreab, W., Hauzenberger, C. A., Johnson, P. R., Kusky, T. M., and Macey, P.: Orogen styles in the East African Orogen: a review of the Neoproterozoic to Cambrian tectonic evolution, J. Afr. Earth Sci., 86, 65–106, https://doi.org/10.1016/j.jafrearsci.2013.06.004, 2013.

Fubelli, G., Abebe, B., Dramis, F., and Vinci, S.: Geomorphological evolution and present-day processes in the Dessie Graben (Wollo, Ethiopia), Catena, 75, 28–37, https://doi.org/10.1016/j.catena.2008.04.001, 2008.

Ganas, A., Pavlides, S., and Karastathisa, V.: DEM-based morphometry of range-front escarpments in Attica, central Greece, and its relation to fault slip rates, Geomorphology, 65, 301–319, https://doi.org/10.1016/j.geomorph.2004.09.006, 2005.

Gao, M., Zeilinger, G., Xu, X., Wang Q., and Hao, M.: DEM and GIS analysis of geomorphic indices for evaluating recent uplift of the northeastern margin of the Tibetan Plateau, China, Geomorphology, 190, 61–72, https://doi.org/10.1016/j.geomorph.2013.02.008, 2013.

Gessesse, D.: Forest Decline in South Central Ethiopia Extent, history and process. Doctoral dissertation. Department of Physical Geography and Quaternary Geology. Stockholm University, Sweden, 2007.

Gete, Z. and Hurni, H.: Implications of Land Use and Land Cover dynamics for mountain resource degradation in the northwestern Ethiopian highlands, Mt. Res. Dev., 21, 184–191, https://doi.org/10.1659/0276-4741(2001)021[0184:IOLUAL]2.0.CO;2, 2001.

Gezahegn, A. and Dessie, T.: Report on Engineering geophysical investigation of the Blue Nile basin for rerouting of the main road, Ethiopian Institute of Geological Survey, Addis Ababa, 1994.

Goitom, B., Oppenheimer, C., Hammond, J. O., Grandin, R., Barnie, T., Donovan, A., Ogubazghi, G., Yohannes, E., Kibrom, G., Kendall, J. M., and Carn, S. A.: First recorded eruption of Nabro volcano, Eritrea, 2011, B. Volcanol., 77, 85, 2015.

Gouin, P.: Kara Kore and Serdo epicenters: relocation and tectonic implications, B. Geophys. Obs., 15, 15–25, 1975.

Gouin, P.: Earthquake history of Ethiopia and the Horn of Africa, International Development Research Centre, Ottawa, Canada, 1979.

Habtamu, E., Ermiyas, F., Tutan, N., and Tsigehana, T.: Engineering Geological Map of Dila Sheet at scale of 1:250,000 scale (NB 37-6), Geological Survey of Ethiopia, Addis Ababa, 2012.

Hayward, N. J. and Ebinger, C. J.: Variations in the along-axis segmentation of the Afar Rift system, Tectonics, 15, 244–257, https://doi.org/10.1029/95TC02292, 1996.

Hearn, G. J.: Slope hazards on the Ethiopian road network, Q. J. Eng. Geol. Hydrogeol., 52, 295–311, 2018.

ISRM, International Society of Rock Mechanics Commission on Testing Methods: Suggested method for determining point load strength, Int. J. Rock Mech. Min. Sci. Geomech., 22, 51–60, https://doi.org/10.1016/0148-9062(85)92985-7, 1985.

Janetos, A. C. and Justice, C. O.: Land covers global productivity: a measurement strategy for the NASA programme, Int. J. Remote Sens., 21, 1491–1512, https://doi.org/10.1080/014311600210281, 2000.

JICA and GSE: The Project for Developing Countermeasures against Landslides in the Abay River Gorge, technical report, Japan International Cooperation Agency and Geological Survey of Ethiopia, Addis Ababa, 348 pp., 2012.

Kopačková, V., Rapprich, V., Sebesta, J., and Zelenkova, K.: Slope dependent morphometric analysis as a tool contributing to re-

construction of volcano evolution, In Earth and environmental sciences, InTech, https://doi.org/10.5772/29466, 2011.

Kropáček, J., Vařilová, Z., Baroň, I., Bhattacharya, A., Eberle, J., and Hochschild, V.: Remote sensing for characterisation and kinematic analysis of large slope failures: Debre sina landslide, main ethiopian rift escarpment, Remote Sens., 7, 16183–16203, https://doi.org/10.3390/rs71215821, 2015.

Kumar, V., Gupta, V., and Sundriyal, Y. P.: Spatial interrelationship of landslides, litho-tectonics, and climate regime, Satluj valley, Northwest Himalaya, Geol. J., 54, 537–551, https://doi.org/10.1002/gj.3204, 2019.

Kycl, P., Rapprich, V., Verner, K., Novotný, J., Hroch, T., Mišurec, J., Eshetu, H., Haile, E. T., Alemayehu, L., and Goslar, T.: Tectonic control of complex slope failures in the Ameka River Valley (Lower Gibe Area, central Ethiopia): Implications for landslide formation, Geomorphology, 288, 175–187, https://doi.org/10.1016/j.geomorph.2017.03.020, 2017.

Lemessa, G., Asfaw, B., Mamo, S., and Ashenafi, S.: Mass movement hazards assessment on Betto and Sawla sub sheet of Goffa district, North Omo Zone, Southern Nations Nationalities and People's Regional State, technical Report, Geological Survey of Ethiopia, Addis Ababa, 2000.

Mancini, F., Ceppi, C., and Ritrovato, G.: GIS and statistical analysis for landslide susceptibility mapping in the Daunia area, Italy, Nat. Hazards Earth Syst. Sci., 10, 1851–1864, https://doi.org/10.5194/nhess-10-1851-2010, 2010.

Meinhardt, M., Fink, M., and Tünschel, H.: Landslide susceptibility analysis in central Vietnam based on an incomplete landslide inventory: Comparison of a new method to calculate weighting factors by means of bivariate statistics, Geomorphology, 234, 80–97, https://doi.org/10.1016/j.geomorph.2014.12.042, 2015.

Melese, S. M.: Effect of land use land cover changes on the forest resources of Ethiopia, International Journal of Natural Resource Ecology and Management, 1, 51, https://doi.org/10.11648/j.ijnrem.20160102.16, 2016.

Muluneh, A. A., Cuffaro, M., and Doglioni, C.: Left-lateral transtension along the Ethiopian Rift and constrains on the mantle-reference plate motions, Tectonophysics, 632, 21–31, https://doi.org/10.1016/j.tecto.2014.05.036, 2014.

Peduzzi, P.: Landslides and vegetation cover in the 2005 North Pakistan earthquake: a GIS and statistical quantitative approach, Nat. Hazards Earth Syst. Sci., 10, 623–640, https://doi.org/10.5194/nhess-10-623-2010, 2010.

Pike, R. J.: Geomorphomery-diversity in quantitative surface analysis, Prog. Phys. Geogr., 24, 1–20, https://doi.org/10.1177/030913330002400101, 2000.

Rapprich, V. and Eshetu, H.: Geological hazards and engineering geology maps of Dilla NB 37-6, Czech Development Agency, Czech Geological Survey, Geological Survey of Ethiopia, Addis Ababa, 2014.

Rapprich, V., Erban, V., Fárová, K., Kopačková, V., Bellon, H., and Hernandez, W.: Volcanic history of the Conchagua Peninsula (eastern El Salvador), J. Geosci., 55, 95–112, https://doi.org/10.3190/jgeosci.069, 2010.

Rapprich, V., Nida, D., and Bizuye, Y.: Geological hazards and engineering geology maps of Hossana NB 37-2, Czech Development Agency, Czech Geological Survey, Geological Survey of Ethiopia, Addis Ababa, 2014.

Saria, E., Calais, E., Stamps, D. S., Delvaux, D., and Hartnady, C. J. H.: Present-day kinematics of the East African Rift, J. Geophys. Res.-Sol. Ea., 119, 3584–3600, https://doi.org/10.1002/2013JB010901, 2014.

Sembroni, A., Faccenna, C., Becker T. W., Molin, P., and Abebe, B.: Long-term, deep-mantle support of the Ethiopia-Yemen Plateau, Tectonics, 35, 69–488, https://doi.org/10.1002/2015TC004000, 2016.

Tadesse, T.: Recent landslide and resulting damages in the Blue Nile River Gorge and its tributaries, Eastern Gojam Zone, Technical Report, Geological Survey of Ethiopia, Addis Ababa, 1993.

Temesgen, B., Umer, M., Asrat, A., Berakhi, O., Ayele, A., Francesco, D., and Demissie, M.: Landslide hazard on the slopes of Dabicho Ridge, Wondo Genet area: the case of June 18, 1996 event, SINET: Ethiopian Journal of Science, 22, 127–140, 1999.

Temesgen, B., Mohammed, M. U., and Korme, T.: Natural hazard assessment using GIS and remote sensing methods, with particular reference to the landslides in the Wondogenet area, Ethiopia, Phys. Chem. Earth Pt. C, 26, 665–675, https://doi.org/10.1016/S1464-1917(01)00065-4, 2001.

U.S. Geological Survey: Earthquake Hazards Program, Advanced National Seismic System (ANSS), Comprehensive Catalogue of Earthquake Events and Products: Various, https://doi.org/10.5066/F7MS3QZH, 2017.

Vařilová, Z., Kropáček, J., Zvelebil, J., Šťastný, M., and Vilímek, V.: Reactivation of mass movements in Dessie graben, the example of an active landslide area in the Ethiopian Highlands, Landslides, 12, 985–996, https://doi.org/10.1007/s10346-015-0613-2, 2015.

Verner, K., Megerssa, L., Buriánek, D., Martínek, K., Hroch, T., Yakob, M., Haregot, A., Bewketu, H., Mosisa, A., Dalke, G., Hejtmánková, P., and Krejčí, Z.: Geological map at a scale of 1 : 50 000, Geological and thematic maps at a scale of 1:50,000 for Mejo, Leku, Arba Minch and Dila areas, SNNPR, Ethiopia. Czech Geological Survey, Prague, Map Sheet 0638-D2 Mejo, 2018a.

Verner, K., Megerssa, L., Hroch, T., Buriánek, D., Martínek, K., Gebremariyam, H., Tadesse, E., Legesse, F., Nisra, E., Abateneh, B., Hejtmánková, P., and Krejčí, Z.: Geological map at a scale of 1 : 50 000, Geological and thematic maps at a scale 1 : 50 000 for Mejo, Leku, Arba Minch and Dila areas, SNNPR, Ethiopia, Czech Geological Survey, Prague, Map Sheet 0637-D3 Arba Minch, 2018b.

Verner, K., Megerssa, L., Hroch, T., Buriánek, D., Martínek, K., Janderková, J., Šíma, J., Kryštofová, E., Gebremariyam, H., Tadesse, E., Legesse, F., Nisra, E., Abateneh, B., Assefa, G., Valenta, J., Pécskay, Z., Hejtmánková, P., and Krejčí, Z.: Explanatory notes to the thematic geoscientific maps of Ethiopia at a scale of 1 : 50 000, Czech Geological Survey, Prague, Map Sheet 0637-D3 Arba Minch, 2018c.

Verner, K., Megerssa, L., Hroch, T., Buriánek, D., Martínek, K., Yakob, M., Haregot, A., Janderková, J., Šíma, J., Kryštofová, E., Valenta, J., Bewketu, H., Mosisa, A., Dalke, G., Assefa, G., Pécskay, Z., Hejtmánková, P., and Krejčí, Z.: Explanatory notes to the thematic geoscientific maps of Ethiopia at a scale of 1 : 50 000, Czech Geological Survey, Prague, Map Sheet 0638-D2 Mejo, 2018d.

Wilks, M., Ayele, A., Kendall, J. M., and Wookey, J.: The 24th January 2016 Hawassa earthquake: Implications for seismic haz-

ard in the Main Ethiopian Rift, J. Afr. Earth Sci., 125, 118–125, https://doi.org/10.1016/j.jafrearsci.2016.11.007, 2017.

Williams, F. M., Williams, M. A. J., and Aumento, F.: Tensional fissures and crustal extension rates in the northern part of the Main Ethiopian Rift, J. Afr. Earth Sci., 38, 183–197, https://doi.org/10.1016/j.afrearsci.2003.10.007, 2004.

Woldearegay, K.: Review of the occurrences and influencing factors of landslides in the highlands of Ethiopia: With implications for infrastructural development, Momona Ethiopian Journal of Science, 5, 3–31, https://doi.org/10.4314/mejs.v5i1.85329, 2013.

Woldegabriel, G., Heiken, G., White, T. D., Asfaw, B., Hart, W. K., and Renne, P. R.: Volcanism, tectonism, sedimentation, and the paleoanthropological record in the Ethiopian Rift System, Special papers-Geological Society of America, 83–99, 2000.

Wolfenden, E., Ebinger, C., Yirgu, G., Deino, A., and Ayale, D.: Evolution of the northern Main Ethiopian rift: birth of a triple junction, Earth Planet. Sc. Lett., 224, 213–228, https://doi.org/10.1016/j.epsl.2004.04.022, 2004.

Wood, J. D.: The geomorphologic characterization of digital elevation models, PhD Thesis, University of Leicester, UK, 1996.

Wotchoko, P., Bardintzeff, J. M., Itiga, Z., Nkouathio, D. G., Guedjeo, C. S., Ngnoupeck, G., Dongmo, A., and Wandji, P.: Geohazards (Floods and Landslides) in the Ndop Plain, Cameroon volcanic nine, Open Geosci., 8, 429–449, https://doi.org/10.1515/geo-2016-0030, 2016.

Xue, L., Alemu, T., Gani, N. D., and Abdelsalama, M. G.: Spatial and temporal variation of tectonic uplift in the southeastern Ethiopian Plateau from morphotectonic analysis, Geomorphology, 309, 98–111, https://doi.org/10.1016/j.geomorph.2018.02.025, 2018.

Yekoye, B., Yewubinesh, B., and Debebe, N.: Engineering Geological Map of Hosaina sheet (NB 37-2) at scale of 1 : 250 000, Geological Survey of Ethiopia, Addis Ababa, 2012.

Zvelebil, J., Šíma, J., and Vilímek, V.: Geo-risk management for developing countries – vulnerability to mass wasting in the Jemma River Basin, Ethiopia, Landslides, 7, 99–103, https://doi.org/10.1007/s10346-009-0191-2, 2010.

Zwaan, F. and Schreurs, G.: Rift segment interaction in orthogonal and rotational extension experiments: Implications for the large-scale development of rift systems, J. Struct. Geol., 140, 1–17, https://doi.org/10.1016/j.jsg.2020.104119, 2020.